A Pattern Fusion Algorithm to Determine the Effectiveness of Predictions of Respiratory Surrogate Motion Multiple-Steps Ahead of Real Time

by

Irene Zawisza

Graduate Program of Medical Physics
Duke University

Date: _____

Approved:

_____
Fang-Fang Yin, Supervisor

_____
Lei Ren

_____
Robert Reiman

_____
David Yoo

Thesis submitted in partial fulfillment of the requirements for the degree of
Master of Science in the Graduate Program of Medical Physics
in the Graduate School of Duke University
2015

Abstract

A Pattern Fusion Algorithm to Determine the Effectiveness of Predictions of Respiratory Surrogate Motion Multiple-Steps Ahead of Real Time

by

Irene Zawisza

Graduate Program of Medical Physics
Duke University

Date: _____

Approved:

_____
Fang-Fang Yin, Supervisor

_____
Lei Ren

_____
Robert Reiman

_____
David Yoo

An abstract of a thesis submitted in partial fulfillment of the requirements for the degree of Master of Science in the Graduate Program of Medical Physics in the Graduate School of Duke University
2015

Abstract

Purpose: Ensuring that tumor motion is within the radiation field for high-dose and high-precision radiosurgery in areas greatly influenced by respiratory motion. Therefore tracking the target or gating the radiation beam by using real-time imaging and surrogate motion monitoring methods are employed. However, these methods cannot be used to depict the effect of respiratory motion on tumor deviation. Therefore, an investigation of parameters for method predicting the tumor motion induced by respiratory motion multiple steps ahead of real time is performed. Currently, algorithms exist to make predictions about future real-time events, however these methods are tedious or unable to predict far enough in advance.

Methods and Materials: The algorithm takes data collected from the Varian RPM^{TM} System, which is a one-dimensional (1D) surrogate signal of amplitude versus time. After the 1D surrogate signal is obtained, the algorithm determines on average what an approximate respiratory cycle is over the entire signal using a rising edge function. The signal is further dividing it into three components: (a) training component is the core portion of the data set which is further divided into subcomponents of length equal to the input component; (b) input component serves as the parameter searched for throughout the training component, (c) analysis component used as a validation against the prediction. The prediction algorithm consists of three major steps: (1) extracting top-ranked subcomponents from training component which best-match the input component; (2) calculating weighting factors from

these best-matched subcomponents; (3) collecting the proceeding optimal subcomponent and fusing them with assigned weighting factors to form prediction. The prediction algorithm was examined for several patients, and its performance is assessed based on the correlation and root mean square error (RMSE) between prediction and known output.

Results: Respiratory motion data was simulated for 30 cases and 555 patients and phantoms using the RPM system. Simulations were used to optimize prediction algorithm parameters. The simulation cases were used to determine optimal filters for smoothing and number of top-ranked subcomponents to determine optimal subcomponents for prediction. Summed difference results in a value of 0.4770 for the 15 Point Savitzky-Golay filter.

After determining the proper filter for data preprocessing the number of required top-ranked subcomponents for each method was determine. Equal Weighting has a maximum average correlation, $c = 0.997$ when using 1 Subcomponent, Relative Weighting has a maximum average correlation, $c = 0.997$ when using 2 Subcomponents, Pattern Weighting has a maximum average correlation $c = 0.915$ when using 1 subcomponent, Derivative Equal Weighting has a maximum average correlation $c = 0.976$ when using 2 Subcomponents, and Derivative Relative Weighting has a maximum average correlation of $c = 0.976$ when using 5 Subcomponents.

The correlation coefficient and RMSE of prediction versus analysis component distributions demonstrate an improvement during optimization for simulations. This is true for both the full and half cycle prediction. However, when moving to the clinical data the distribution of prediction data, both correlation coefficient and RMSE, there is not an improvement as the optimization occurs. Therefore, a comparison of the clinical data using the 5 Pt moving filter and arbitrarily chosen number of subcomponents was performed. In the clinical data, average correlation coefficient between prediction and analysis component 0.721 ± 0.390, 0.727 ± 0.383, 0.535 ± 0.454,

0.725 ± 0.397, and 0.725 ± 0.398 for full respiratory cycle prediction and 0.789 ± 0.398, 0.800 ± 0.385, 0.426 ± 0.562, 0.784 ± 0.389, and 0.784 ± 0.389 for half respiratory cycle prediction for equal weighting, relative weighting, pattern, derivative equal and derivative relative weighting methods, respectively. Additionally, the clinical data average RMSE between prediction and analysis component 0.196 ± 0.174, 0.189 ± 0.161, 0.302 ± 0.162, 0.200 ± 0.169, and 0.202 ± 0.181 for full respiratory cycle prediction and 0.155 ± 0.171, 0.149 ± 0.138, 0.528 ± 0.179, 0.174 ± 0.150, and 0.173 ± 0.149 for half respiratory cycle prediction for equal weighting, relative weighting, pattern, derivative equal and derivative relative weighting methods, respectively. The half cycle prediction displays higher accuracy over the full cycle prediction. Wilcoxon signed-rank test reveals statistically highly significant values ($p < 0.1\%$) for 4 out of 5 algorithms favoring the half cycle prediction (Equal, Relative, Derivative Equal, and Derivative Relative Weighting Methods). In this method, the relative weighting method has the most correlations coefficients with values greater than 0.9 and also yields the largest number of highest correlations over other prediction methods. **Conclusions:** In conclusion, the number of subcomponents used for prediction may be better deter- mined based on individual breathing pattern. The prediction accuracy using patient data is better using half cycle prediction over full cycle prediction for all algorithms for the majority of methods tested. Finally, relative weighting method performed better than other methods.

Dedicated to the Zawisza Family.

Contents

List of Tables

List of Figures

List of Abbreviations and Symbols

Abbreviations

CBCT	Cone Beam Computed Tomography
CIRS	Computerized Imaging Reference Systems, Inc.
cc	Correlation Coefficient
e	Euclidean Distance
h	Hamming Distance
IGRT	Image Guided Radiation Therapy
MAD	Mean Absolute Deviation
MLC	Multileaf Collimator
NN	Neural Network
RPM	Real-time Position Management^{TM}
RMSE	Root Mean Square Error
S-G	Savitzky-Golay
SBRT	Sterotactic Body Radiation Therapy
SBV	Sliced Body Volume
4D DTS	Four-Dimensional Digital Tomosynthesis

Acknowledgements

I would like to acknowledge the support of my advisors, Dr. Fang-Fang Yin and Dr. Lei Ren from Duke Department of Radiation Oncology. Without their advice and support, I would have not been able to compile this thesis. I would also like to thank my other committee members, Dr. Robert Reiman and Dr. David Yoo, for their time and effort.

I would also like to thank Dr. Hui Yan for his assistance in understanding signal processing and his willingness to share his knowledge in prediction algorithm development. Without his direction, understanding the nature of prediction would not be feasible. Additionally, I would like to thank my peers in Yin Laboratory for the support and advice in algorithm testing and design.

I would like to thank the Department of Radiation Physics and Radiation Oncology at Duke University Medical Center and the Department of Medical Physics at Duke University for research and travel funding.

Finally, I would like to thank my family and friends for their support throughout not only my graduate school career but my scientific career. Without them I could not have been successful.

1

Introduction

Radiation therapy utilizes ionizing radiation with the goal of curing or palliating disease and minimizing damage to healthy tissue. Localization using Image Guided Radiation Therapy (IGRT) is performed in order to ensure tumor location and minimize toxicity of normal tissue due to inaccurate irradiation.[1],[2],[3] IGRT can consist of both radiation sources or non-radiation sources to track the tumor position. For instance, prior to treating lung tumor using SBRT, a CBCT will be taken to localized the tumor. When examining tumors that are in areas affected heavily by motion, such as lung and abdominal cancers, motion management techniques[4],[5],[6],[7],[8] are employed including:

- Respiratory gated radiotherapy [5],[7]
- Tracking

Motion management uses real-time imaging and surrogate monitoring to assure that tumor motion is within the radiation field during high-dose and high-precision radiotherapy.

Real-time imaging methods include audio prompting or visual feedback to create

relatively reproducible breathing patterns.[6] Another technique utilizes internal organ motion tracking, such as of the diaphragm, to reconstruct respiratory motion.[8] Similarly, breath-hold methods require patients to fix their respiratory motion in a specified phase while administering radiation, but this can be troublesome for patients who cannot hold their breath.[7] Other methods include use 4DCT to determine a Sliced Body Volume (SBV) to create a signal similar to an amplitude motion signal.[2] In regions where tumor motion is heavily affected by respiration, radiation gating is used to precisely target the tumor during beam-on time.[9] Respiratory gating radiotherapy requires the administration of radiation at particular points in a patients respiratory phase.[7] Respiratory gating radiotherapy utilizes external signals obtained from systems such as the Real-time Position Management^{TM} (RPM) System, internal signals from systems such as the Calypso Tracking, or external radiation such as fluoroscopy to determine when the radiation beam should be turned on because the tumor is in the field.

These methods are useful in providing real-time tumor/surrogate motion but no future information is available. Future information is necessary to account for feedback delays from signal reception and beam gating, gantry and collimator rotation, and MLC movement, a decision must be made when the beam can be administered for tumor position with accurate beam parameters, thus requiring knowledge about tumor position ahead of real time.[10] Minimizing deviations between actual respiratory motion from the prediction are key in reducing incorrect radiation administration.[4],[11]

1.1 Current Prediction Models

Current models to predict respiratory motion ahead of time use methods such as Fuzzy Analysis[12], Neural Networks[13],[14], circular pattern augmentation[10], and

Multi-Step Linear Methods[15].

1.1.1 Fuzzy Analysis

In Toshabi's Fuzzy Prediction Model, the algorithm requires a user dependent clustering calculation to determine an initial model. The model is updated if it detects an amplitude drift within a specified deviation. When the model must be updated, it retrains the algorithm, therefore requiring longer treatment time. Additionally, the method only performed prediction for 200ms in advance, which is not far enough in advance.

1.1.2 Neural Networks

Other methods utilize Neural Networks (NN) to create a data base of patterns and possible predictions. NN require a certain learning speed to create such a database. In Yan's technical study using a NN, surgical clips were required to determine if internal motion can be predicted from external markers. The study uses multiple markers and several data must be developed to produce a complex network for prediction. Additionally, as samples for predictions were increased over $\approx$6 seconds there was a noticeable negative effect on the correlation between predicted signal and internal signal and the predicted error between the prediction and internal signal. Similarly, Seregni's feasibility study uses a NN to track tumors but the final outcome has some amplitude errors which reach up to 5mm, which is insufficient for high-precision radiosurgery[7].

1.1.3 Circular Pattern Augmentation

Hong's methods use angular velocity and circular motion to make predictions. The circular nature of respiratory motion is exhibited by the CIRS phantom and replicating this in respiratory prediction seems obvious. However, Hong only attempts to

make predictions for 0.4 s, which would only account for RPM system latencies and would be inefficient for radiosurgery.[10]

1.1.4 Multi-Step Linear Methods

The studies Ernst is of particular interest because it is relatively simple model to make predictions. Uses linear modeling to predict RPM system delays. Ernst only predicts external system delays of approximately 15 samples or 150 ms.[15]

1.1.5 Pattern Fusion

Pattern fusion prediction is novel because it has been considered for cloud storage prediction and update forecasting and will now be applied for tracking and gating prediction. Pattern fusion will take previously collected data from a patient surrogate signal to fuse together creating a prediction. Surrogate motion position is adequate information because demonstrated previously is strong correlation between internal position and external surrogate markers.[16]

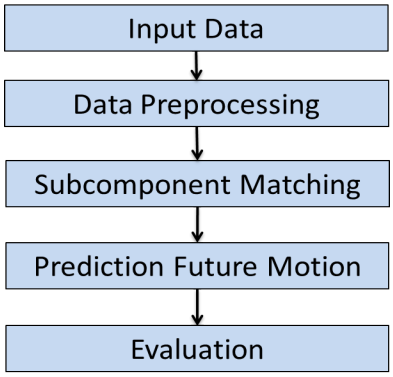

FIGURE 1.1: General Prediction Algorithm Workflow.

The prediction algorithm workflow has been designed based on Yang et. al. "A Pattern Fusion Model for Multi-Step-Ahead CPU Load Prediction."[17] The algorithm workflow is depicted in Figure 1.1 as a flowchart. Each step in the algorithm

will be described in detail in Chapters 2 through 6.

1.2 Hypothesis

The pattern fusion algorithm will make predictions at most one respiratory cycle (approximately 3 to 6 seconds), with a user dependent decision on prediction length. Predictions will be made quickly and require no retraining. There is no need to update the metrics because the prediction is based on a fixed data input.

Figure 1.2, describes the pros and cons of each method and suggests what should be accomplished using the novel pattern fusion algorithm.

	Fuzzy Analysis	Neural Network	Circular Pattern Augmentation	Multi-Step Linear	Pattern Fusion
Time to Form Prediction	Long	Long	Short	Short	Short
Prediction Length	Short	Long	Short	Short	Unknown
Retraining Necessary	Yes	Yes	No	No	No

FIGURE 1.2: General Prediction Algorithm Workflow.

1.3 Aim

To track the target location precisely by developing and investigating a pattern fusion algorithm for multiple-step ahead prediction.

2

Materials

From Figure 1.1, the first step of the prediction algorithm is to Input Data. Input Data has a workflow that is depicted in Figure 2.1.

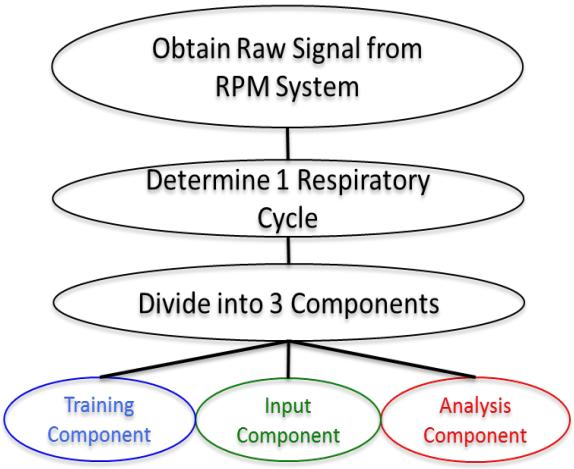

FIGURE 2.1: Input Data Workflow

2.1 Real-time Position Management^{TM} System

Duke University Medical Center Department of Radiation Oncology uses the RPM System to track respiratory motion and provide real time-imaging. The RPM System

uses an infrared tracking system via a respiratory block, pictured in Figure 2.2, to acquire a 1D signal of respiratory amplitude over time. Data can be tracked continuously at 30 Hz.[18],[19] By using a continuously tracked amplitude signal, tumor location and motion can be reproduced and multi-step ahead prediction can be performed.[3],[4]

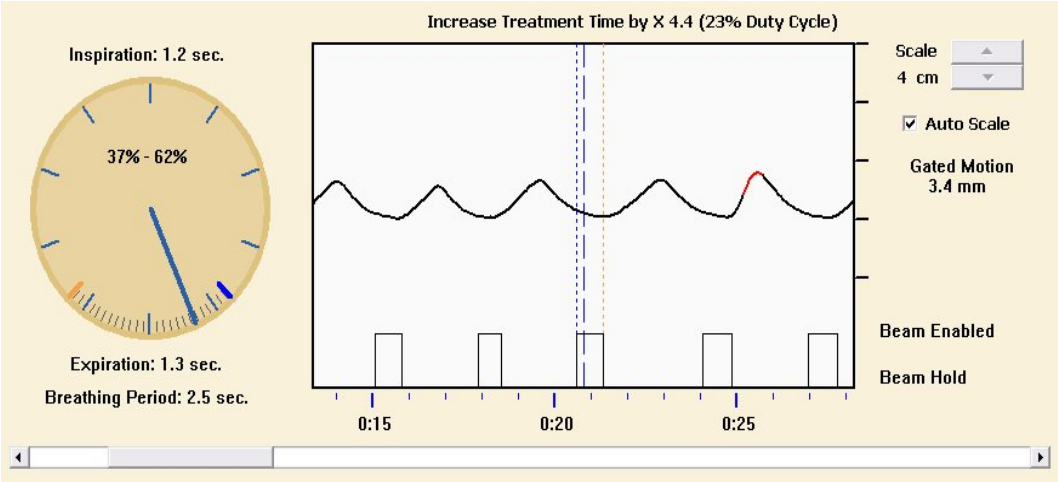

FIGURE 2.2: RPM User Interface. Image courtesy of Varian[18],[19].

2.2 Input Data

The algorithm takes data collected from the Varian RPM^{TM} System (See Figure 2.2), which is a one-dimensional (1D) surrogate signal of amplitude versus time. After the 1D surrogate signal is obtained, the algorithm determines on average what an approximate respiratory cycle is over the entire signal using a rising edge function. The signal is further dividing it into three components:

1. Training Component
2. Input Component
3. Analysis Component

where the input and analysis components are approximately 1 respiratory cycle, as determined in the second step of the Input Data. The training component is generally the core portion of the data set which is further divided into subcomponents of length equal to the input component. This process of using subcomponents will be described in more complete detail in Chapter 4. The input component serves as the parameter searched for throughout the training component. Finally, the analysis component is used for comparison against the prediction. Within the algorithm, the analysis component will be truncated from the data in order to offer no information when making a prediction. These components are illustrated in a patient signal in Figure 2.3.

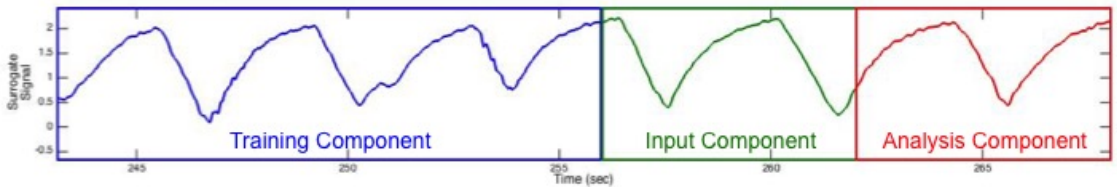

FIGURE 2.3: Data Components as part of the Input Data step in the prediction algorithm. In blue is the Training Component, green is the Input Component, and in red is the Analysis Component.

In Chapters 3-5, we will further describe the Methods of Preprocessing, Subcomponent Matching, and Prediction Methods used in the prediction algorithm.

3

Data Preprocessing

In Chapter 2, the raw signal was broken down into its 3 components through Data Input. In Figure 1.1, the next step in the algorithm is Data Preprocessing. The goal of data preprocessing is to manipulate the data into a more practical form. Figure 3.1 shows the general workflow of data preprocessing.

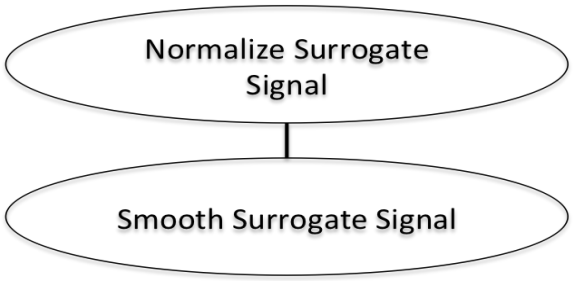

FIGURE 3.1: Data Preprocessing Workflow

First, the signal is normalized to its minimum and maximum values. Figure 3.2 shows a raw surrogate signal. The effect of normalization on this signal is demonstrated in Figure 3.3.

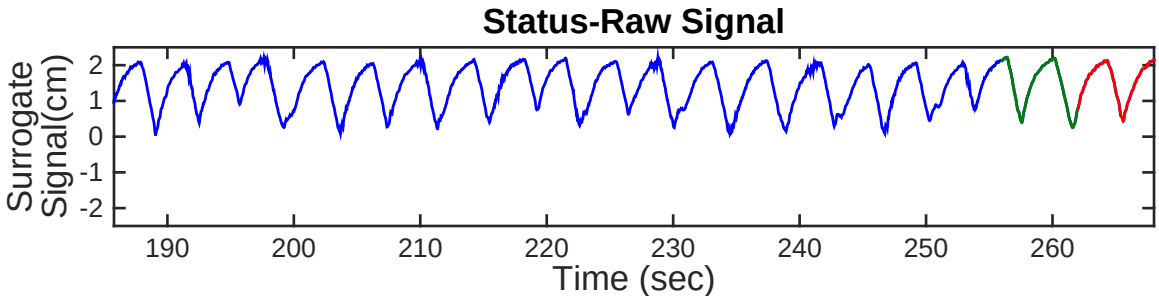

FIGURE 3.2: Raw Surrogate Signal

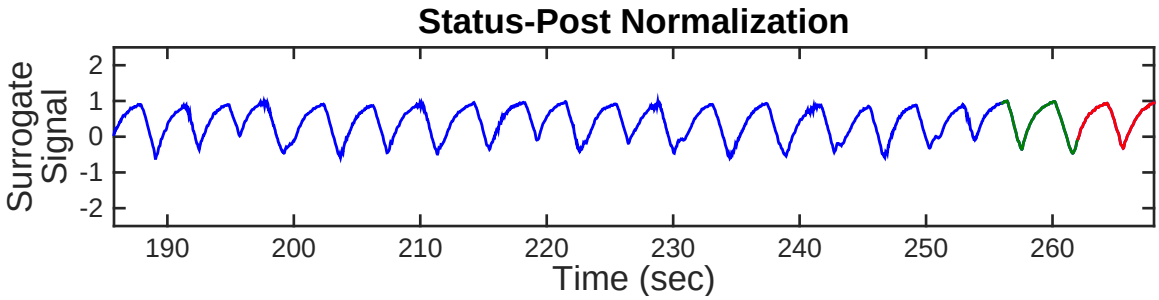

FIGURE 3.3: Normalized Surrogate Signal. Signal normalized to minimum and maximum values

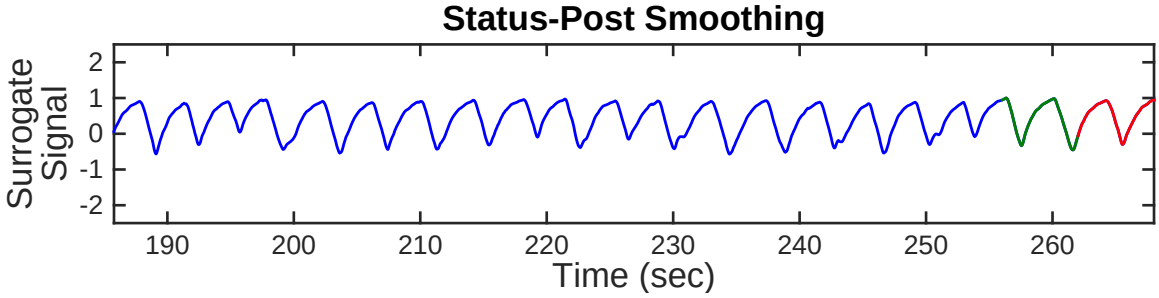

FIGURE 3.4: Smoothed and Normalized Surrogate Signal. Smoothing performed using 15 Point Savitzky-Golay Filter.

After normalization is performed, and before a respiratory data set can be entered into a prediction algorithm, the data should be smoothed to discriminate noise while still maintaining the integrity of the original signal. The original algorithm, prior to optimization, utilized a 5 point moving filter for smoothing. Figure 3.4 demonstrates

the effect of smoothing on the same normalized signal using a 15 Point Savitzky-Golay Filter. The following filters were examined to determine the optimal filter for an automated prediction algorithm:

- Moving Filter
- Savitzky-Golay Filter

These filters will now be discussed in greater detail below.

3.1 Moving Filter

The moving filter uses a moving average over a number of points, or span. It takes the average of the neighboring points in an input span. This is similar to a low pass filter with an output given by

$$y_s(i) = \frac{1}{2N+1}(y(i+N) + y(i+N-1) + ... + y(i-N)) \tag{3.1}$$

The span, N, is the number of points over which a filter will operate. For the moving filter, an odd span must be used in order to have the smoothing occur at the center point, i, of the span. The end points are not able to be smoothed because there is no defined span. The moving filter tends to filter out high frequency content. A Moving 5 point span is the default smoothing filter in Matlab. However, because the data input for the prediction is generally very long with 30Hz sampling, a 5 point span may have a minimal effect of smoothing. [20]

3.2 Savitzky-Golay (S-G) Filter

S-G filters are similar to moving filters in that they weight the ratio in Equation 3.1 using coefficients that preserve higher frequency data. The S-G filter operates using:

$$y_s(i) = \sum_{n=-n_L}^{n_R} c_n y_{i+n} \tag{3.2}$$

where n_L is the number of points used to the left of the central point, i, and n_R is the number of points to the right of the central point. Then the span of the filter, N, at any given location in the data is composed of n_L to n_R and is the total number of points that smoothing will occur over. Here c_n is the filter coefficient preserving the higher frequency data via higher order polynomials. Then at each point y_i there is a polynomial fit performed over the corresponding span. Then $y_s(i)$ is the value of the polynomial at position i and none of the other values are used. This is process is iterated across the entire data set. [21]

4

Subcomponent Matching

In Chapter 3, the data was manipulated to a more practical form through Data Preprocessing. According to Figure 1.1, the next step in the algorithm is Subcomponent Matching. The goal of subcomponent matching is to identify which parts of training component best match to input component, so that the next subcomponent can be used as the optimal subcomponent believed to best match the analysis component. Figure 4.1 shows the general workflow of subcomponent matching.

The first step in subcomponent matching, is to divide the training component into subcomponents that are in equal length to the input component. Iterating through every subcomponent in the training component, the algorithm searches for subcomponents that are similar to the input component. Searching is performed using three parameters

- Correlation Coefficient (cc)
- Hamming Distance (h)
- Euclidean Distance (e)

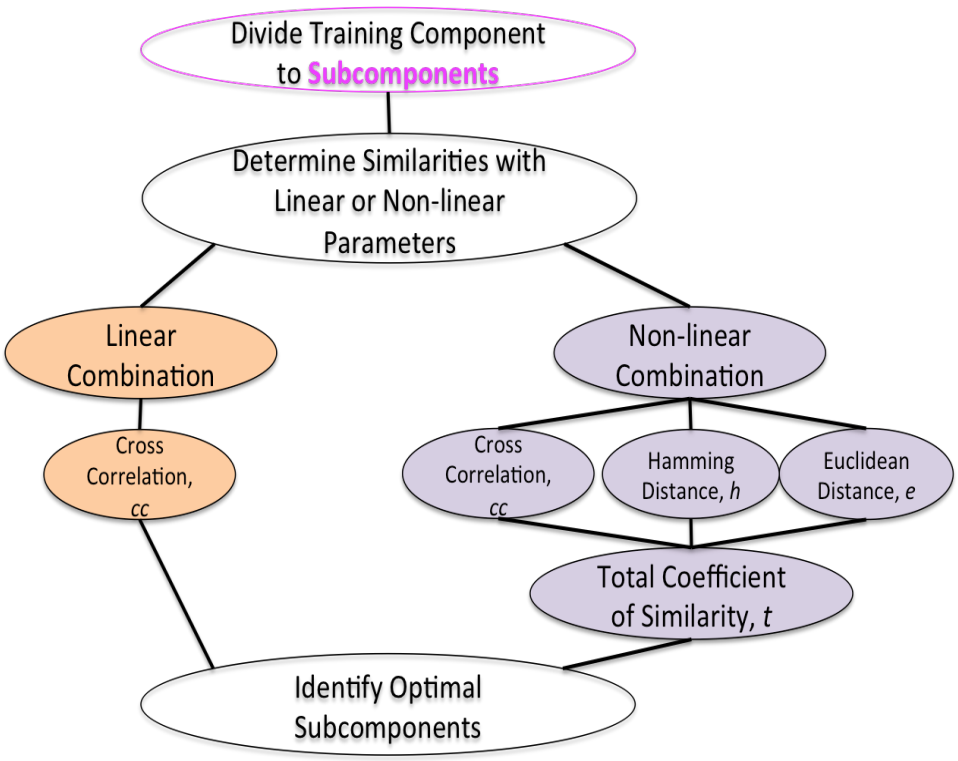

FIGURE 4.1: Workflow of Subcomponent Matching. Notice that the left uses linear combinations to determine similarities (highlighted in orange) and on the right uses non-linear combinations to determine similarities (highlighted in purple).

4.1 Correlation Coefficient

Correlation coefficient, cc, quantifies the similarity and dependence between the input component and each subcomponent or how closely the mean values are related. The correlation coefficient is mathematically defined as the ratio of the expectation value between two components to the standard deviations of these two components, or:

$$cc = \frac{\sum_i (X_i - \bar{X})(Y_i - \bar{Y})}{(\sum_i (X_i - \bar{X})^2)^{\frac{1}{2}} (\sum_i (Y_i - \bar{Y})^2)^{\frac{1}{2}}} \tag{4.1}$$

where in our case X_i would be the subcomponent ,represented by A in Figure 4.2 over all points i in the subcomponent, or as averaged over the entire subcomponent $\bar{X}$, and Y_i and Y is the input component represented by B in Figure 4.2 over all

points i in the input component, or as averaged over the entire input component, $\bar{Y}$. A cc value of 1 is perfectly correlating, while a value of 0 has no correlation, and a value of -1 is oppositely correlating.[22]

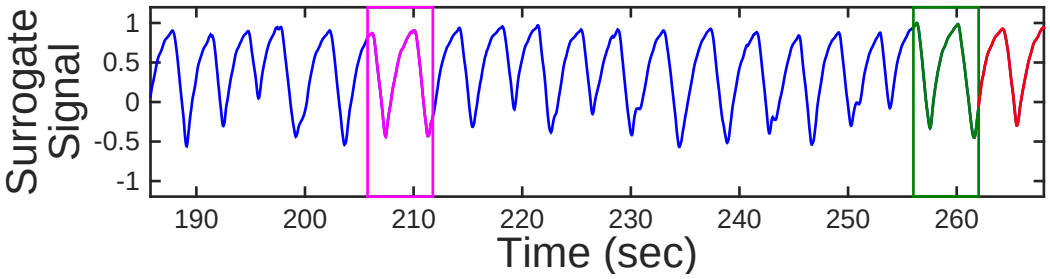

FIGURE 4.2: Subcomponent is represented in magenta by A for a patient signal. Input component is represented in green by B.

4.2 Hamming Distance

The Hamming Distance, h represents the slope changes between the subcomponent and the input component. The first step to calculate h is to find the fluctuation pattern for each component. Any descending portions of the signal receive a value of -1 and ascending portions of the signal receive a value of 1. Mathematically, the signal fluctuation, sf is written as

$$sf = \begin{cases} 1 & i < i+1 \\ -1 & i > i+1 \end{cases} \tag{4.2}$$

The fluctuation is calculated for the subcomponent and the input component. In Figure 4.3, the subcomponent is A and its fluctuation is C and the input component is B and its fluctuation is D. The next step is to take the absolute difference between the fluctuation patterns. In Figure 4.3, this is mathematically represented by $|C - D|$ and is depicted in E. Then the final hamming distance is calculated as:

$$h = 1 - \frac{\sum E}{N} \tag{4.3}$$

where E is the absolute difference in the fluctuation in signals and N is the length of the input component.

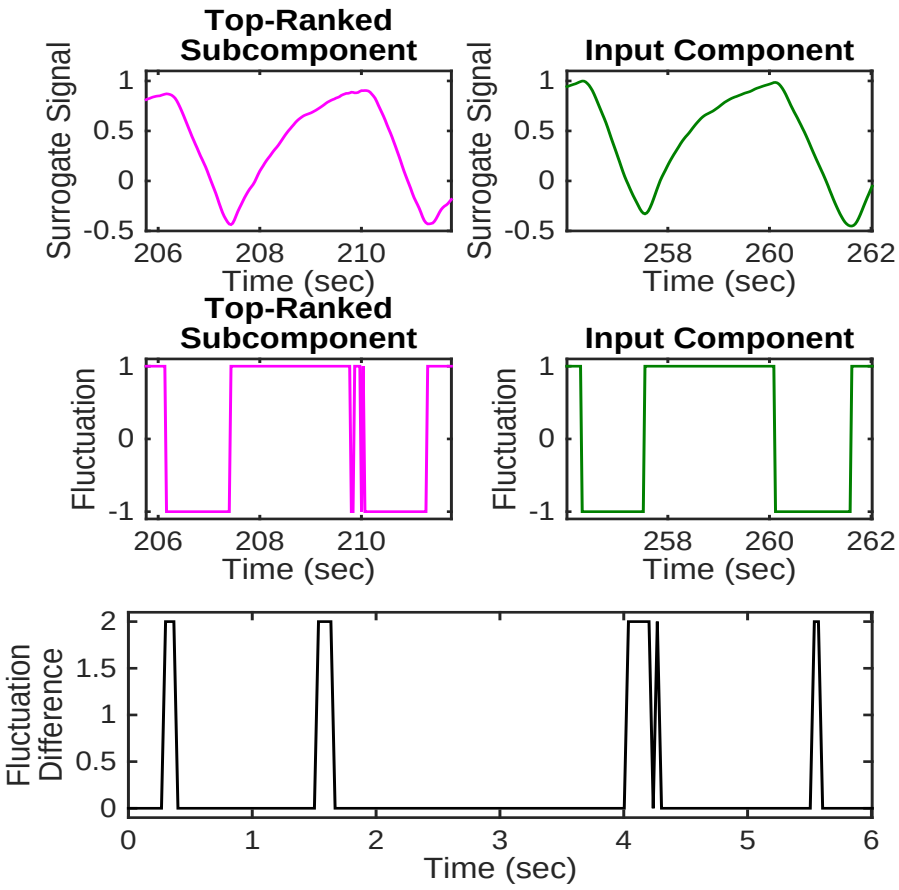

FIGURE 4.3: Signal Fluctuation Representation. From Figure 4.2, the subcomponent calculations are on the left by figures A and C and the Input component calculations are on the right by figures B and D. The absolute difference between the fluctuations is represented in E.

4.3 Euclidean Distance

Euclidean distance, e, represents the amplitude changes between the subcomponent and input component. It is the sum of the absolute difference between the subcom-

ponent and input component, mathematically as:

$$e = \sum_i |X - Y| \tag{4.4}$$

where from Figure 4.2 X is the subcomponent and Y is the input component. Visually, the Euclidean distance is represented in Figure 4.4 by the blue lines.

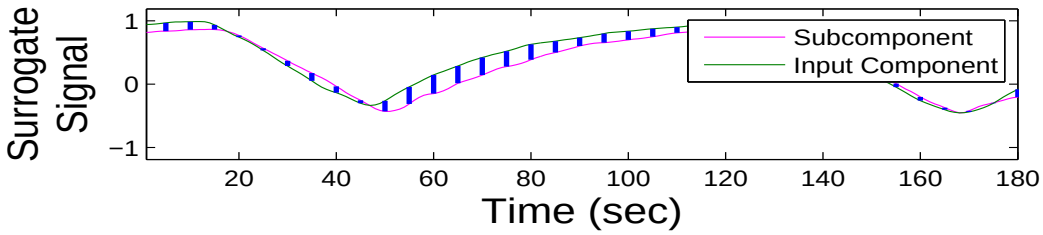

FIGURE 4.4: Illustration of the Euclidean Distance. From Figure 4.2, the subcomponent is represented in magenta by A for a patient signal and the Input component is represented in green by B.

4.4 Linear Combinations

Then based upon the model, either a linear or non-linear combination is used to determine the top-ranked subcomponents and optimal subcomponents. Linear combinations take the form:

$$y = c_0 + c_1 x + c_2 x^2 + \dots \tag{4.5}$$

where the c terms are constants and x terms are parameters determined by the given model. In this algorithm, the linear combination uses a single metric, correlation coefficient, to begin identifying the top-ranked subcomponents.

After calculating the *cc* of every subcomponent, the values are ordered in a descending order to obtain the most similar subcomponents. These top-ranked subcomponents are selected with the only requirement of separation from all other top-ranked subcomponents by a designated separation distance, which is the length of the input and analysis components. If these patterns are separated by a value less

than this distance, they are removed and the next best candidate is selected. This is done in order to prevent choosing successive subcomponents.

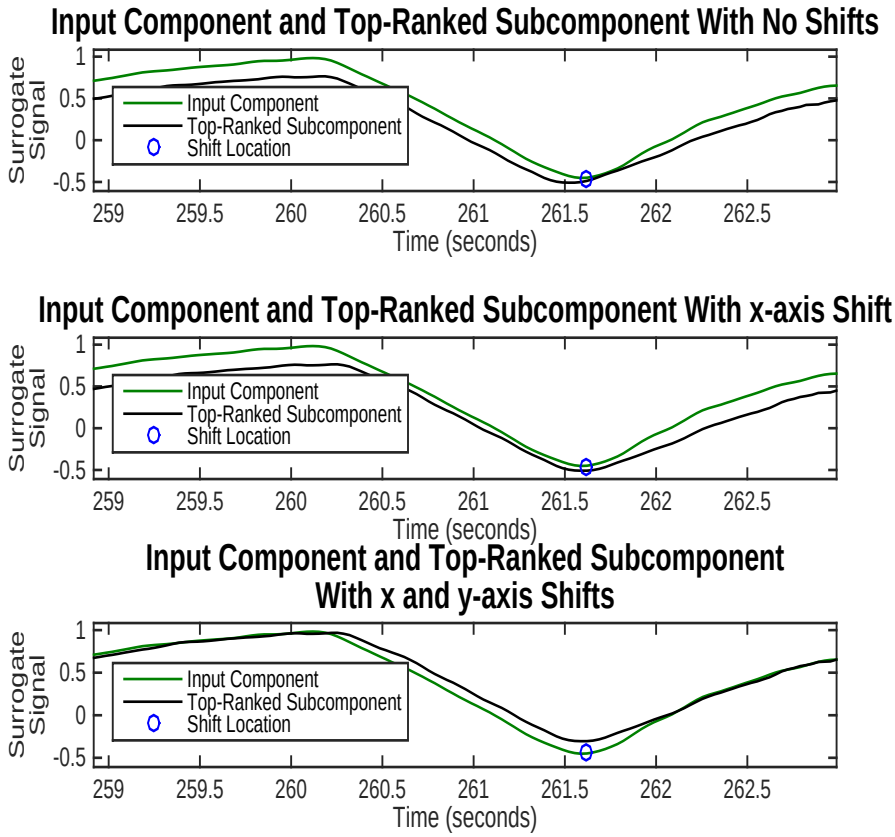

FIGURE 4.5: Linear Combination Signal Matching.

Finally, the peak and trough magnitudes are identified on the input component (Figure 4.5 Top) and the one of greatest magnitude is marked as the point where the similar point in the top-ranked component will be shifted to match (Figure 4.5 Middle). Then the final motion point of the input component is found and the top-ranked component is matched to this point (Figure 4.5 Bottom). The motion matching is performed so that the first point of the prediction will match the motion

of the analysis component. The shifts are recorded and applied to the optimal subcomponents before being sent to prediction. (See Section Optimal Subcomponents)

4.5 Non-linear Combinations

Non-linear combinations use correlation coefficient, Hamming Distance, and Euclidean Distance of a given subcomponent to identify similarities between subcomponents and the input component. While non-linear combinations can take on many forms indicating that the criteria is not linear, in this case the non-linear combination criteria for selection is the total coefficient of similarity, t, calculated as:

$$t = \frac{cc \cdot h}{e} \tag{4.6}$$

While this is one way to calculate the total coefficient of similarity, in the future other methods could be considered.

After calculating the t of every subcomponent, the values are ordered in a descending order to obtain the top ranked subcomponents. A separation metric is calculated that the top-ranked subcomponents should remain a length equal to the input and analysis component apart from one another in order to prevent successive selection of top-ranked subcomponents. Any lower ranked subcomponents that are a distance less than this distance are removed from the ranks and the next candidate is selected.

4.6 Optimal Subcomponents

After the top-ranked subcomponents are identified, the optimal subcomponents are the subcomponents immediately proceeding those top-ranked subcomponents and are chosen for fusion because they are believed to most closely represent the analysis

component. In Figure 4.6, the top-ranked components for a patient signal can be seen in magenta and the optimal subcomponents can be seen in black.

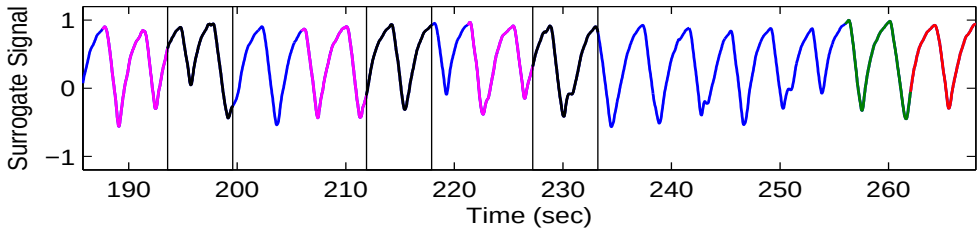

FIGURE 4.6: Top-ranked subcomponents can be seen in magenta. The optimal subcomponents are the subcomponents immediately following the top ranked subcomponents and can be seen in black. The optimal subcomponents are believed to most closely represent the analysis component see in red.

5

Prediction Method

In Chapter 4, the optimal subcomponents were determined and are believed to best match the analysis component. Now from Figure 1.1, the next step in the algorithm is Predict Future Motion. The purpose of this step is to combine the optimal subcomponents to make a motion prediction.

It is important to note that the linear and non-linear combinations differ in their selection of optimal subcomponents, but often the fusion of to form prediction is the same. While their names will be different this is for identification purposes only. Linear combination predictions (orange) include Derivative Equal Weighting and Derivative Relative Weighting methods. Non-linear combination predictions (purple) are Equal Weighting, Relative Weighting and Pattern Method. Each of these methods are displayed with their respective combination methods in Figure 5.1

5.1 Linear Combinations

Derivative Equal Weighting and Derivative Relative Weighting both use linear combinations for selection of the optimal subcomponents. As seen in Chapter 4, optimal subcomponents are identified and sent for prediction, completing the first step in Fig-

ure 5.1. In these methods the top 6 subcomponents are used for prediction. These two methods differ in their weighting of the subcomponents to make the prediction.

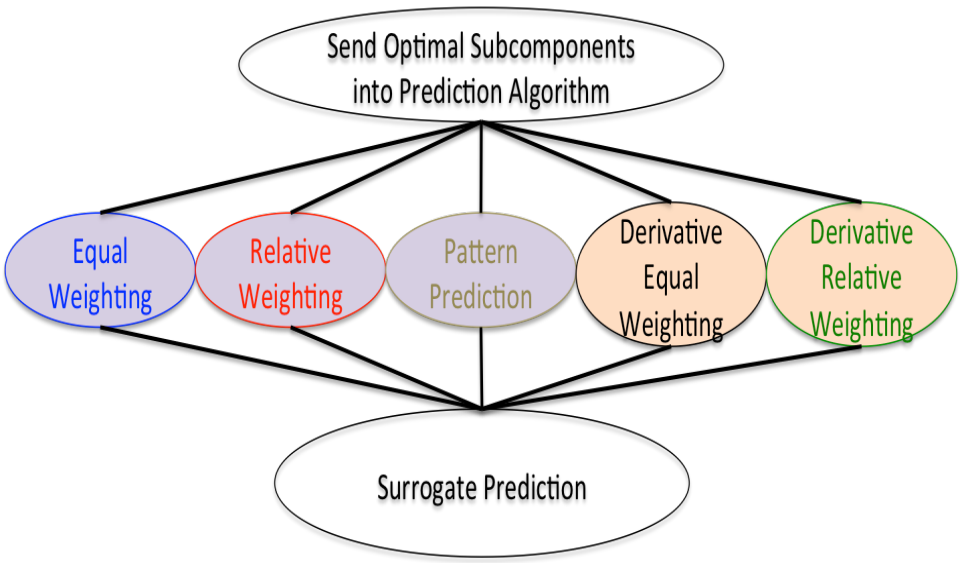

FIGURE 5.1: Prediction Method Workflow. Notice that the three methods on the left are highlighted in purple indicating they are utilizing non-linear combinations to determine similarities and the two methods on the right are highlighted in orange indicating they are utilizing linear combinations to determine similarities.

5.1.1 Derivative Equal Weighting

Derivative Equal Weighting uses equal weighting, or the ratio of the summed optimal subcomponents to the total number of subcomponents used. Mathematically,

$$p = \frac{\sum_i^N s_i}{N} \tag{5.1}$$

where p is the proposed prediction, s_i is the i-th optimal subcomponent, and N is the number of subcomponents used, which in this case $N = 6$.

5.1.2 Derivative Relative Weighting

Derivative Relative Weighting uses relative weighting, or the ratio of the top-ranked subcomponent correlation to the sum of the top-ranked subcomponent correlations

as the weight. Mathematically,

$$w_i = \frac{c_i}{\sum_i^N c_i} \tag{5.2}$$

where c_i is the i-th top ranked subcomponent correlation and N is the number of subcomponents, which in this case $N = 6$. Then the prediction is the summed weight of the subcomponents,

$$p = \sum_i^N w_i s_i \tag{5.3}$$

where p is the prediction, w_i is the i-th weighting factor, and s_i is the i-th subcomponent.

5.2 Non-linear Combinations

The non-linear combination selection of optimal subcomponents applies to Equal, Relative and Pattern Weighting Predictions. As seen in Chapter 4, optimal subcomponents are identified and sent for prediction, completing the first step in Figure 5.1. Recall, that these methods differ from the linear combinations in the way optimal subcomponents are selected.

5.2.1 Equal Weighting

The equal weighting strategy performs similarly to Derivative Equal Weighting. It chooses its 6 optimal subcomponents using the total coefficient of similarity, t, and then uses Equation 5.1 to calculate a prediction. For example, in Figure 5.2 in the top the black optimal subcomponents highlighted in orange will be fused for prediction using Equal weighting.

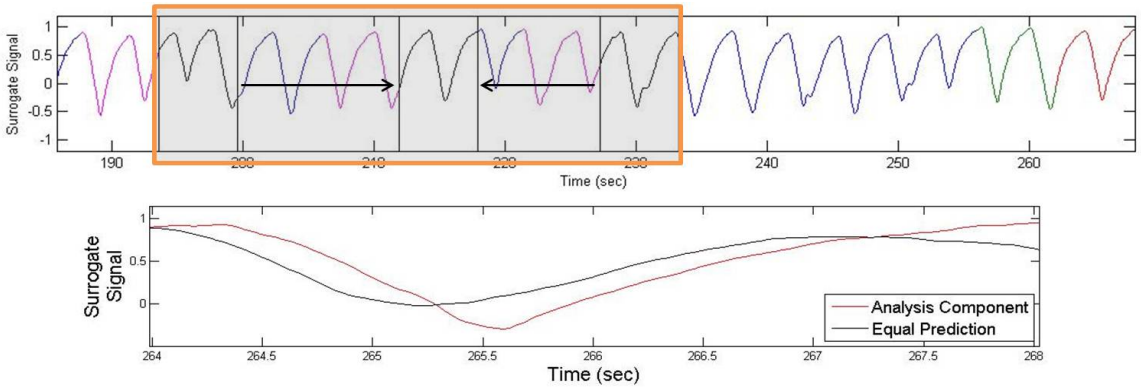

FIGURE 5.2: Fusion of Optimal Subcomponents for Prediction using Equal Weighting. Top from Chapter 4 the Optimal Subcomponents (black) will be fused (orange) to make a prediction, here using equal weighting. Bottom the fused subcomponents form the prediction (black) to be compare to the analysis component (red).

5.2.2 Relative Weighting

Relative Weighting performs similarly to Derivative Relative Weighting. It chooses its 6 optimal subcomponents using the total coefficient of similarity, t. Then the total coefficient of similarity is used to calculate the weighting factor, such that

$$w_i = \frac{c_i}{\sum_i^N t_i} \tag{5.4}$$

where t_i is the i-th top ranked subcomponent total coefficient of similarity and N is the number of subcomponents, which in this case $N = 6$. Then the prediction is the summed weight of the subcomponents, and uses Equation 5.2 to calculate a prediction.

5.2.3 Pattern Weighting

Pattern weighting uses 10 optimal subcomponents found via the total coefficient of similarity, t. The algorithm calculates the baseline shift, amplitude change, and period of the input signal and attempts to manipulate the values for each top-ranked subcomponent to match the input component, applying any corrections to the corresponding optimal subcomponent.

Phase shift is calculated by finding the cross covariance between the input component and a top-ranked subcomponent correlating to its optimal subcomponent. Then it calculates the maximum of this covariance and records the phase shift value and moves the top-ranked subcomponent location (time-position) to this maximum value. This phase shift will then be applied to the optimal subcomponent.

The period is calculated for the optimal phase shifted subcomponents by finding the gradient and calculating its minimums and maximums, i.e. gradient=0, which we will identify as the zero-crossing points. If there are less than 20 samples between the next zero-crossing point, it removes that crossing point and considers that it was some small fluctuation in the signal. Then the periodicity change, ϕ_i, is calculated between each top-ranked subcomponent and input component to be applied to the final optimal subcomponent.

To calculate the baseline shift and amplitude change, the mean, minimum, maximum, and standard deviation of a top-ranked phase shifted component is calculated. The baseline correction, ϵ_i, is computed as the ratio of the standard deviation of the input component to the standard deviation of the top-ranked phase shifted subcomponent. The signal amplification, δ_i, is calculated as the difference in average of the top-ranked phase shifted subcomponent from the input component.

These correction factors are applied to manipulate the optimal subcomponent for use in prediction via

$$s_i = s_i + \phi_i \cdot \epsilon_i + \delta_i \tag{5.5}$$

where s_i is the i-th subcomponent, ϕ_i is the periodicity correction for the i-th subcomponent, ϵ_i is the i-th subcomponent baseline correction, and δ_i is the i-th subcomponent signal amplification.

These corrected optimal subcomponents are fused using Equal weighting via Equation 5.1 to calculate a prediction for $N = 10$ subcomponents.

5.3 Surrogate Prediction

The final step in the prediction is the surrogate prediction. While our methods have formed the prediction using the above methods, a final correction is applied to account for any amplitude changes that might occur due to fusion. This is done using a point-slope calculation to determine what the first amplitude point of the prediction should be and a simple y shift is for all points on the prediction.

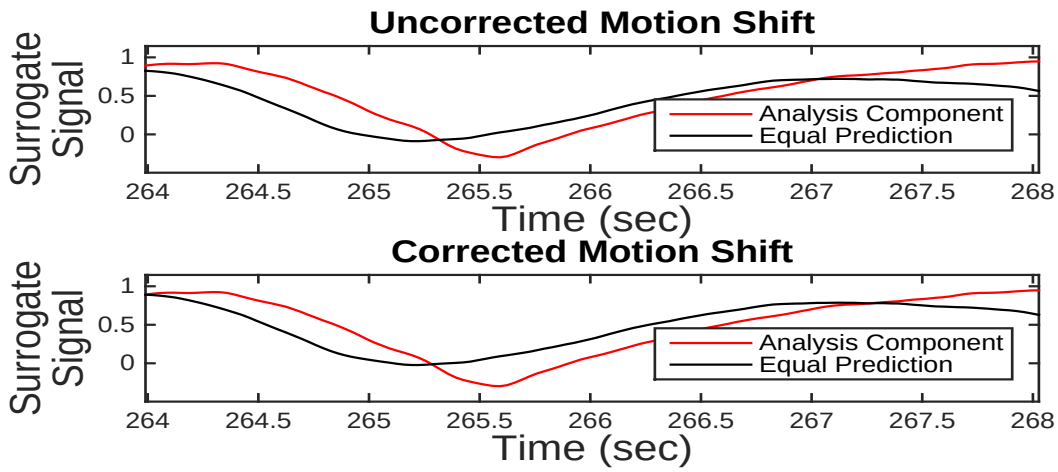

FIGURE 5.3: y-shift correction for surrogate prediction using equal weighting. On top is the uncorrected prediction, and on bottom is the corrected y-shift prediction. The fused subcomponents form the prediction in black to be compare to the analysis component in red.

In Figure 5.3, the top figure represents an equal weighting prediction before motion corrections are made notice the gap between the prediction and analysis at 264 seconds and the bottom figure demonstrates the prediction after the correction is applied notice there is no gap at 264 seconds.

6

Evaluation

The final step in Figure 1.1 is to evaluate the prediction that is being made. This is done using two metrics, cross correlation and root mean square error (RMSE). Cross correlation was described by Equation 4.1. The calculation is the same except it is now being performed between prediction and analysis component. Recall from Chapter 4 that $cc = 1$ represents a perfect correlation, $cc = 0$ represents no correlation, and $cc = -1$ represents a total opposite correlation between the two signals. For example, from a study with 25 surrogate motion cases[23], the correlation coefficient was calculated using the Equal weighting strategy and displayed in Figure 6.1 are the best case and in Figure 6.2 the worst case of prediction based on cross correlation between prediction and analysis component.

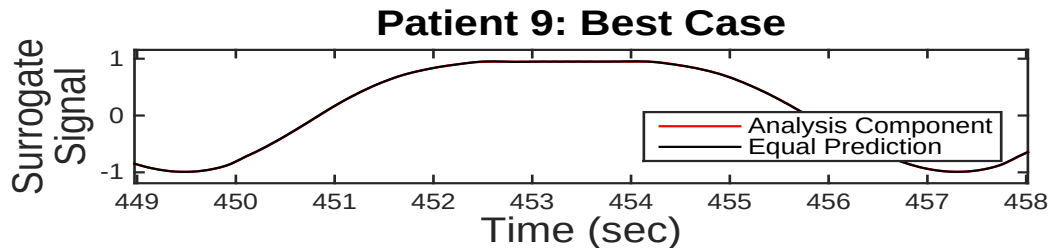

FIGURE 6.1: Best case prediction from [23] using Equal Weighting with a cross correlation $cc = 0.9999$. The analysis component is in red and the prediction is in blue.

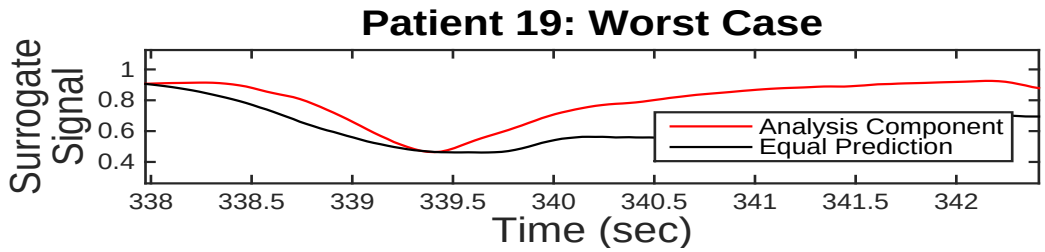

FIGURE 6.2: Worst case prediction from [23] using Equal Weighting with a cross correlation, $cc = 0.4749$. The analysis component is in red and the prediction is in blue.

RMSE is a calculation to determine the overall difference between the prediction points from their average.

$$RMSE = \sqrt{\frac{\sum_i^N (p(i) - a(i))^2}{N}} \tag{6.1}$$

where p is the prediction from a particular algorithm, a is the analysis component from the smoothed and normalized signal, and N is the length of the analysis component. When the RMSE value is close to 0, then it represents a better prediction and when it is close to 1 it represents a poorer prediction.

Using these two metrics the algorithm gets an estimate of how accurate a prediction is compared to what will actually occur.

As the algorithms are developed and run for a multitude of patient cases, to de-

termine if two sets of correlation coefficients and RMSE values have statistically significant differences, a two-sided Wilcoxon signed rank test is performed.

7

Simulations and Clinical Data

7.1 Clinical Data

Duke University Medical Center Department of Radiation Oncology provided a database of 555 patient and phantom surrogate respiratory signals using the RPM System. The resolution of the collected patient data is 0.0333 seconds which corresponds to a frequency of 30 Hz.

7.2 Simulated Signals

In order to determine the optimal parameters to apply to raw surrogate motion data, 30 simulated curves were generated to simulate tumor motion. These curves incorporated some of the following features seen to occur in cancer patients:

- Regular Breathing
- Baseline Shift
- Periodicity Change

- Amplitude Change
- Noisy Breathing

These simulated curves are shown in Figures 7.1-7.5 below. Simulated signals were generated in order to make determinations of the best way to optimize the prediction algorithm. The resolution of the simulated signals is 0.1 seconds which corresponds to a frequency of 10 Hz. When adding noise to patient data, random numbers were generated between 0 and 1 and were then added to the given simulation. The noise metric was chosen such that its effect would be noticeable in the data set and would be comparable to patient data.

It is important to note that due to the syntax of the pattern weighting strategy, the condition of separation in phase by 20 points will not be met when using the simulated signals. Therefore, the phase shift correction will be turned off when making predictions for the simulated signals. However, the phase shift correction will be turned on when making predictions for patient and phantom data.

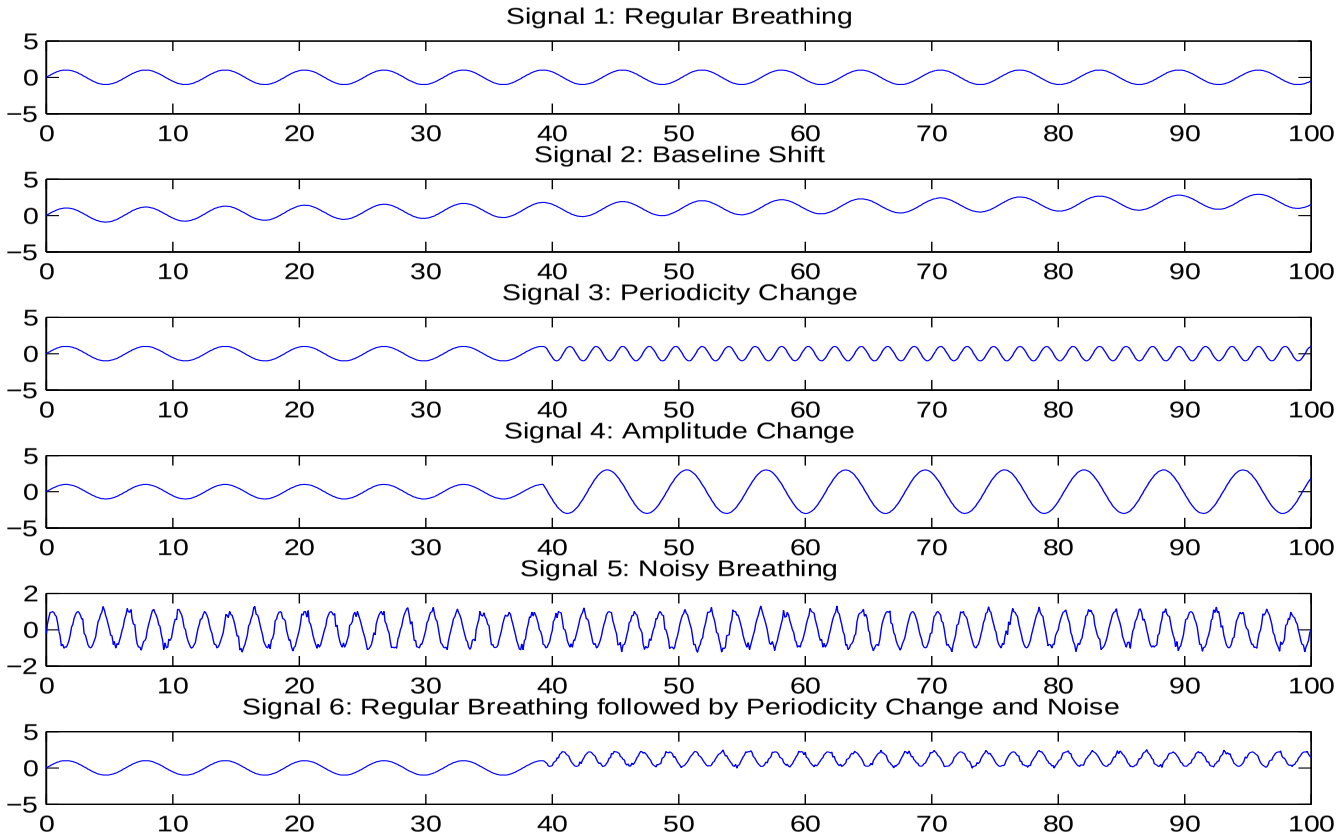

FIGURE 7.1: **Simulated Signals 1 through 6.** Signal 1 regular breathing; Signal 2 baseline shift; Signal 3 periodicity change; Signal 4 amplitude change; Signal 5 noisy breathing; Signal 6 regular breathing followed by periodicity change and noise.

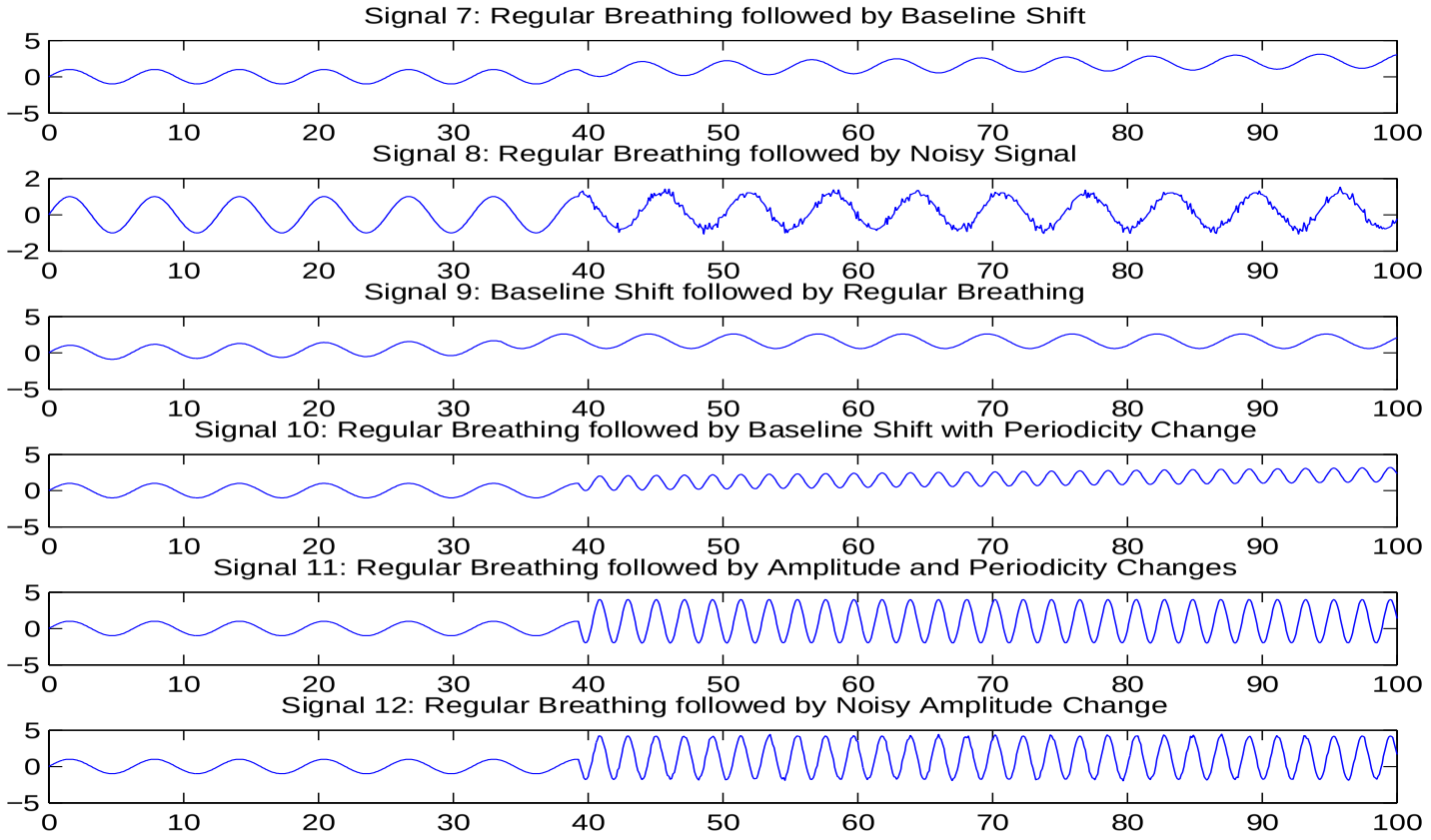

FIGURE 7.2: **Simulated Signals 7 through 12.** Signal 7 regular breathing followed by baseline shift; Signal 8 regular breathing followed by noisy signal; Signal 9 baseline shift followed by regular breathing; Signal 10 regular breathing followed by baseline shift with periodicity change; Signal 11 regular breathing followed by amplitude and periodicity changes; Signal 12 regular breathing followed by noisy amplitude change

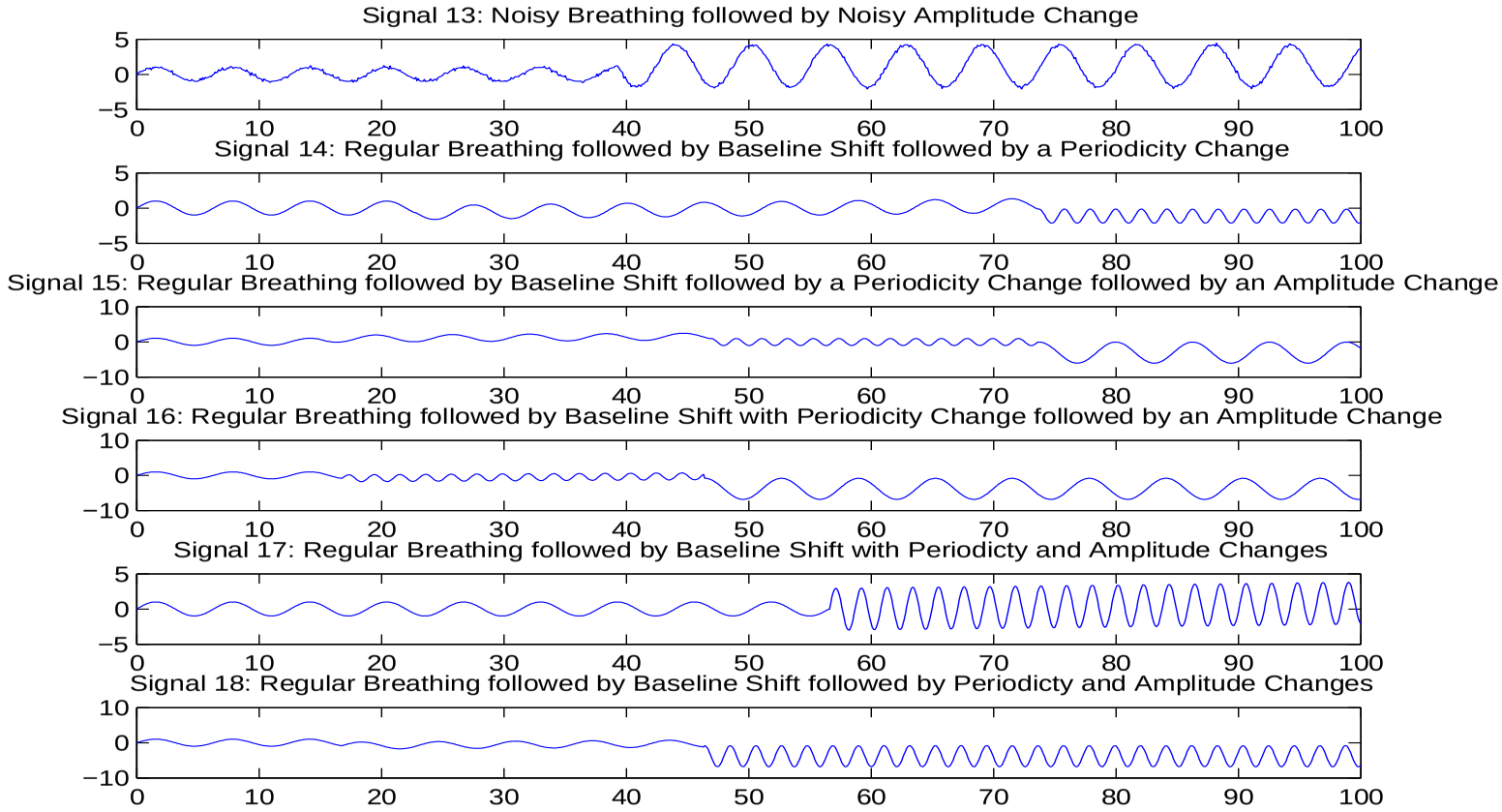

FIGURE 7.3: **Simulated Signals 13 through 18.** Signal 13 noisy breathing followed by noisy amplitude change; Signal 14 regular breathing followed by baseline shift followed by a periodicity change; Signal 15 regular breathing followed by baseline shift followed by a periodicity change followed by an amplitude change; Signal 16 regular breathing followed by baseline shift with periodicity change followed by an amplitude change; Signal 17 regular breathing followed by baseline shift with periodicity and amplitude changes; Signal 18 regular breathing followed by baseline shift followed by periodicity and amplitude changes.

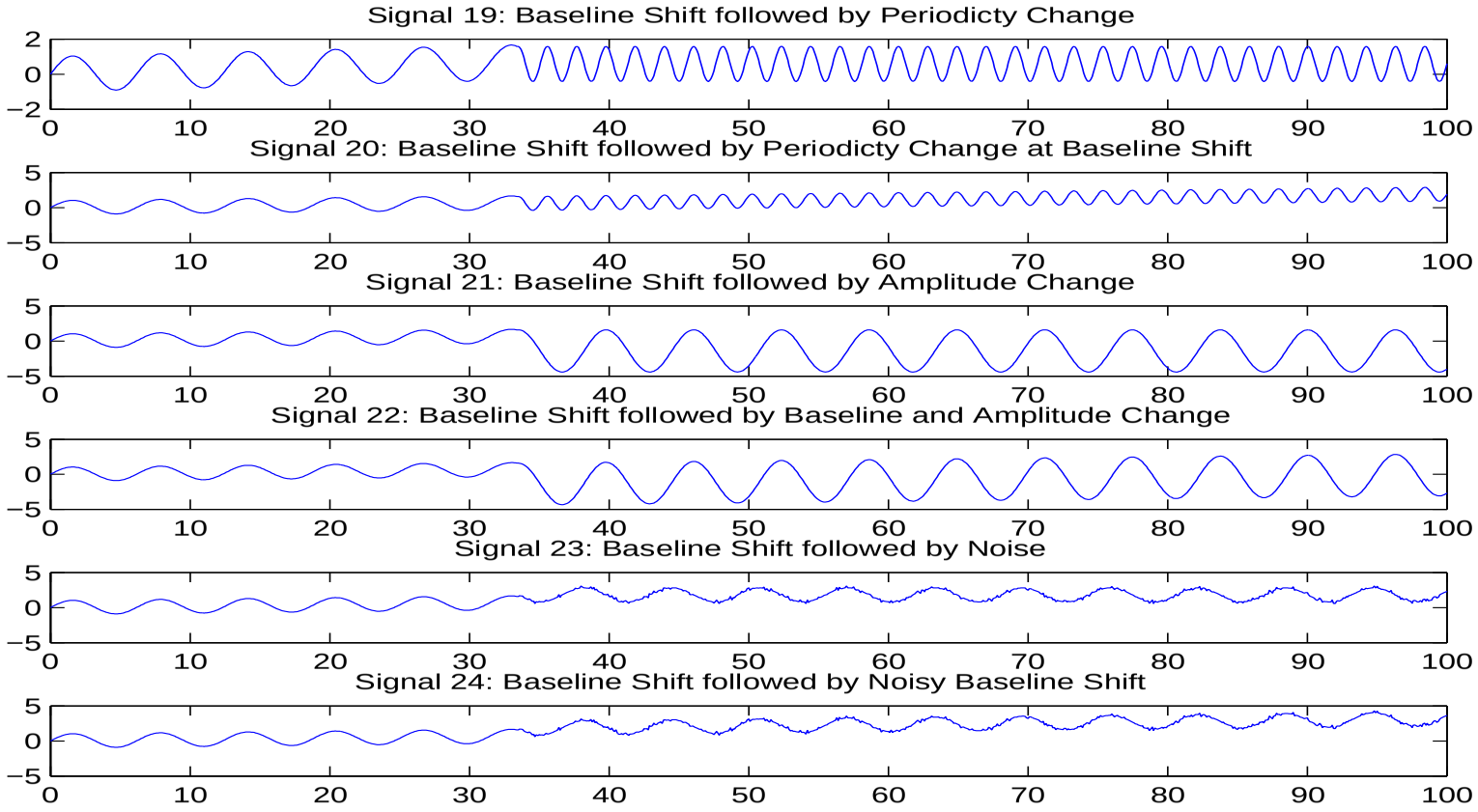

FIGURE 7.4: **Simulated Signals 19 through 24.** Signal 19 baseline shift followed by periodicity change; Signal 20 baseline shift followed by periodicity change at baseline shift; Signal 21 baseline shift followed by amplitude change; Signal 22 baseline shift followed by baseline and amplitude change; Signal 23 baseline shift followed by noise; Signal 24 baseline shift followed by noisy baseline shift.

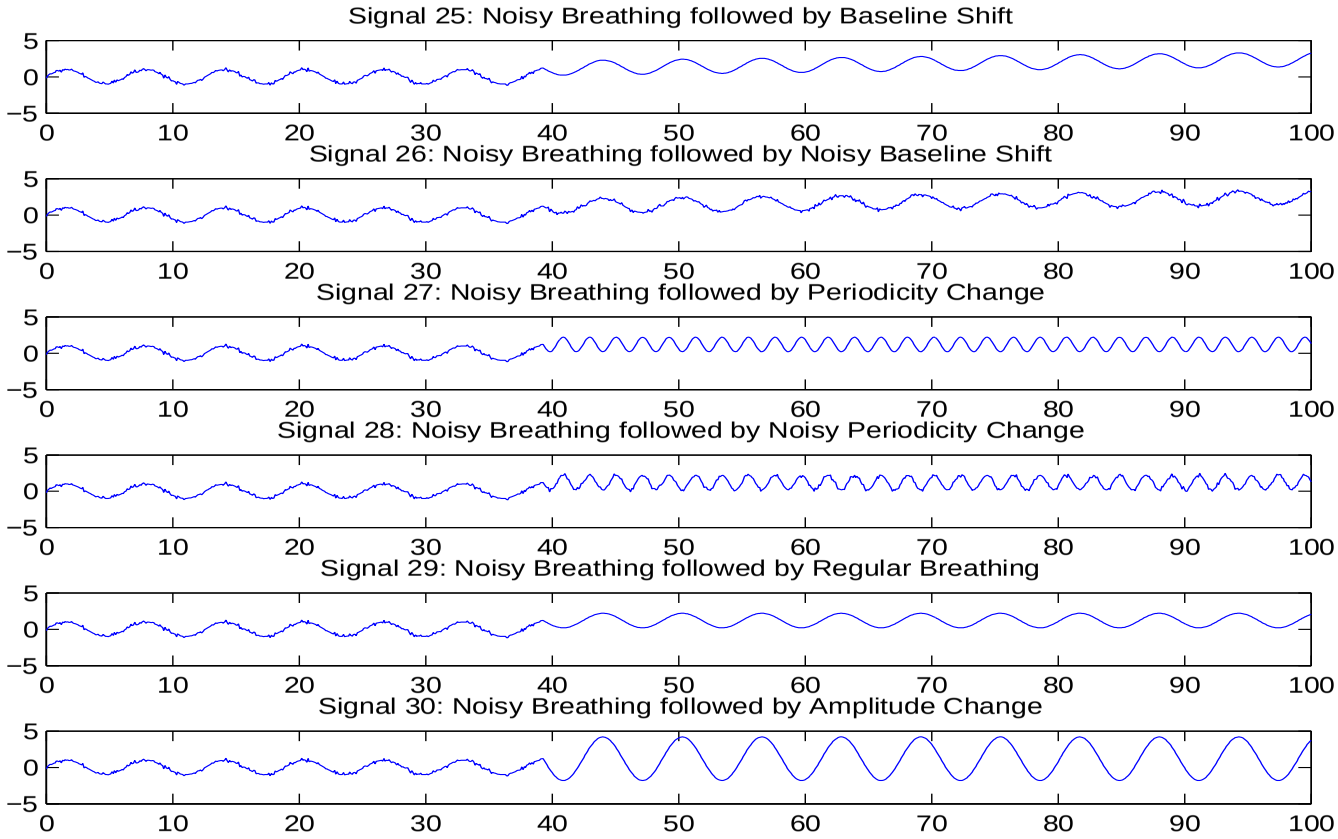

FIGURE 7.5: **Simulated Signals 25 through 30.** Signal 25 noisy breathing followed by baseline shift; Signal 26 noisy breathing followed by noisy baseline shift; Signal 27 noisy breathing followed by periodicity change; Signal 28: noisy breathing followed by noisy periodicity change; Signal 29 noisy breathing followed by regular breathing; Signal 30 noisy breathing followed by amplitude change.

8

Results

8.1 Effect of Smoothing

It is clear that smoothing will affect the outcome of the prediction algorithm, but up to this point, it is undetermined which type of smoothing is deemed best for prediction. Therefore, the aim is to determine an optimal smoothing filter which maintains data integrity but reduces the noise in a surrogate signal. In total, there are 14 types of filters that are discussed in detail in the following sections. The span of smoothing performance for each filter is listed in Table 8.1.

Table 8.1: Smoothing Filter with Respective Number of Points for Smoothing Span.

Smoothing Method:	Moving	Savitzky-Golay
Number of Points Smoothing Span	3, 5, 7, 9, 11, 13, 15	3, 5, 7, 9, 11, 13, 15

As a demonstration of how the smoothing effects the various simulations, the first 6 simulated signals are displayed in Figure 8.1 with a 5 point moving filter and a 15 point S-G filter.

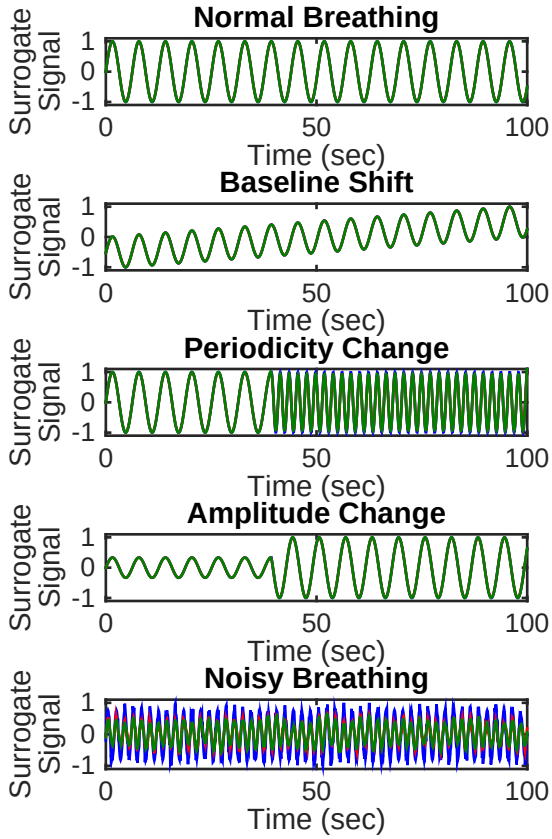

FIGURE 8.1: Smoothing Demonstration on Simulated Signals. Original Simulation in blue. 5 point moving filter in red. 15 point S-G filter in green.

Additionally, the patient signal that has continuously been displayed in Chapters 2 through 6 has a small portion displayed in Figure 8.2 to show give a better picture of how smoothing can filter out noise, but maintain data integrity.

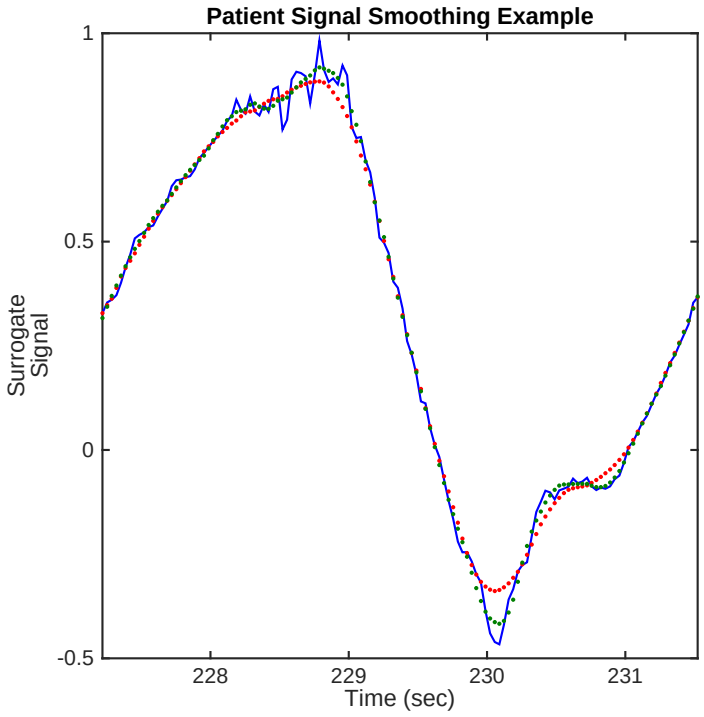

FIGURE 8.2: Smoothing Demonstration on Simulated Signals. Original Simulation in blue. 5 point moving filter in red. 15 point S-G filter in green.

Each filter with the given span was applied to the 30 simulated signals and the correlation coefficient was calculated between the original simulated signal and the smoothed signal. From the distribution of 30 correlation coefficients, to determine an optimal filter which can be used in the prediction algorithm, we can use the following metric

$$S = \Sigma(1 - c_i) \tag{8.1}$$

where S is the summed difference, which is equal to a perfect correlation of 1 minus c_i, or the correlation coefficient between the i-th original simulated signal and the i-th smoothed simulated signal performed for each type of smoothing. The results are depicted in Figure 8.3. Here the moving filter is on the left and S-G is on the right separated by a red bar. For each smoothing method, the span of the smoothing in increasing order. The minimum summed difference metric occurs for S-G 15 Point

Smoothing with a value of $S = 0.4770$.

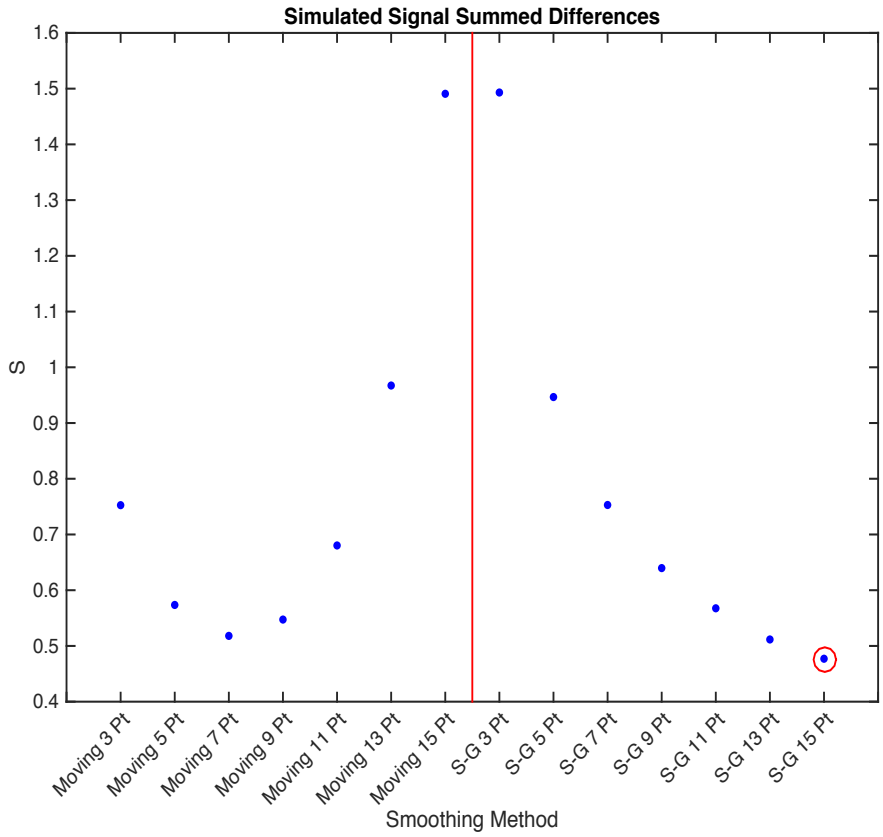

FIGURE 8.3: Summed Difference between Perfect Correlation (1) and Predicted Cross Correlation between 30 Simulated Signals and 14 Types of Smoothing. The red line signifies the change from moving filter to S-G filter. The minimum is circled in red and is located at position 14, or Savitzky-Golay 15 Point Smoothing, with value of 0.4770.

Figure 8.4 further supports the claim that when predictions are performed using the S-G filter, the correlation in the scatter plot are closer to 1 than when a moving filter is used.

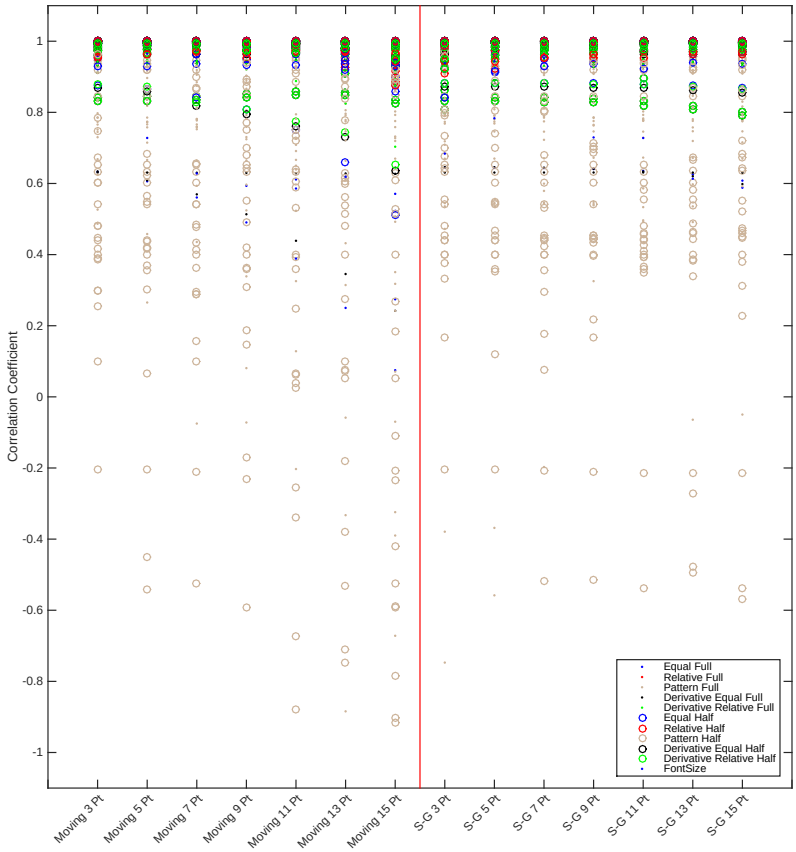

FIGURE 8.4: 30 Simulated Signals Final Correlation Values Between Predictions of Various Methods and (14 Type) Original Smoothed Signal. The red lines signify a change in filter used for smoothing. The columns in each smoothing section are in ascending Span order represented in Table 8.1. The various prediction methods are represented in different colors and the length of the input and analysis component as Full and Half Respiratory Cycle Predictions are represented as dots and circles, respectively.

As seen from Figure 8.2 the S-G 15 point filter does do better than the 5 point moving filter in maintaining data integrity. Therefore, while the original algorithm parameters used a 5 point moving filter, the 15 Point S-G filter is used for Data Preprocessing as algorithm optimization is being performed.

8.2 Effect of Number of Subcomponents

Optimal subcomponents are used for pattern fusion is performed to make a prediction. While the optimal number of subcomponents to make the best prediction possible is unclear, it is clear that number of subcomponents used will affect the outcome of the prediction algorithm, and using more subcomponents could potentially cost computation speed. Therefore, the aim is to determine the optimal number of subcomponents to use for each prediction method to make a prediction.

8.2.1 Equal Weighting Prediction

Figure 8.5 examines the effect of varying the number of optimal subcomponents used for the Equal Weighting Prediction by displaying the final correlation coefficient between the prediction and analysis component (y-axis). The x-axis represents a givens simulation and each number of subcomponent used for prediction is in a different color. Few cases utilize too many subcomponents and the correlations drift from 1. In Simulations 14 and 15, there is a noticeable drop in the final correlation. Recall, Simulation Signal 15 was Regular Breathing followed by Baseline Shift followed by Periodicity Change followed by an Amplitude Change. Notice that the larger number of subcomponents used for this case, the worse the final correlation is. Table 8.2 is a summary of all averages and standard deviations of final correlations and RMSE values, as well as, information depicting where the correlations lie numerically, and which methods have the highest correlation for the given number of subcomponents versus other prediction methods. Notice in bold using 1 subcomponent demonstrate a high final correlation and low RMSE with small variations. Similarly, all simulations have $cc > 0.9$ and 27 of the cases obtain the highest cc value using 1 subcomponent.

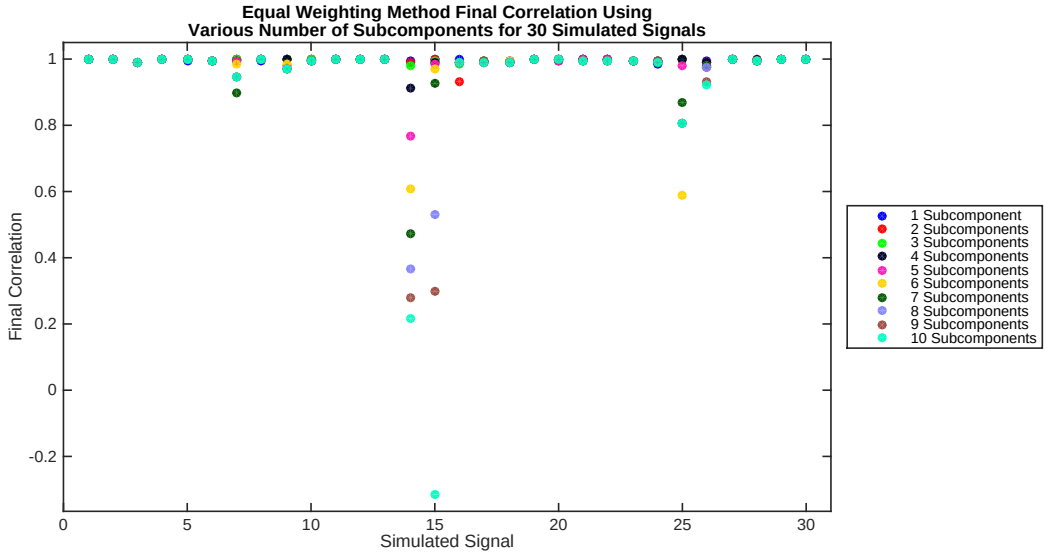

FIGURE 8.5: Output Correlation Values for Equal Weighting Prediction Algorithm for 1 to 10 Subcomponents used for Prediction of 30 Simulated Cases.

Table 8.2: Average and Standard Deviation of Prediction Final Correlations and RMSE, Correlation Classification, and Highest Correlation for 30 Simulated Cases for Approximate Full Respiratory Cycle using Various Number of Subcomponents for Equal Weighting Strategy.

Subcomponents	1	2	3	4	5	6	7	8	9	10
Average Correlation	**0.997**	0.995	0.996	0.994	0.987	0.967	0.968	0.950	0.938	0.915
St. Dev. Correlation	**0.004**	0.012	0.006	0.016	0.042	0.101	0.098	0.143	0.180	0.274
Average RMSE	**0.036**	0.059	0.057	0.078	0.107	0.115	0.121	0.122	0.137	0.156
St. Dev. RMSE	**0.031**	0.109	0.080	0.114	0.129	0.140	0.145	0.146	0.149	0.153
$cc \geqslant 0.9$	**30**	**30**	**30**	30	29	28	27	27	27	27
$0.5 \leqslant cc < 0.9$	0	0	0	0	1	2	2	2	1	1
$cc < 0.5$	0	0	0	0	0	0	1	1	2	2
Highest Correlation	**27**	6	7	9	5	7	7	10	9	8

8.2.2 Relative Weighting Prediction

Figure 8.6 depicts the effect on final correlation coefficient by varying the number of optimal subcomponents using Relative Weighting Prediction. There is very little spreading of the correlations from 1. Simulations 26 has the most spread in correlation. Recall, Simulation Signal 26 was Noisy Breathing followed by Noisy Baseline Shift. Notice that the larger number of subcomponents used for this case, the worse

the final correlation is. Table 8.3 is a summary of all averages and standard deviations of final correlations and RMSE values, as well as, information depicting where the correlations lie numerically, and which methods have the highest correlation for the given number of subcomponents versus other prediction methods. Notice that for relative weighting, a maximum average correlation is obtained with 1 to 8 subcomponents with small RMSE values for subcomponents 1 to 3 (in bold). For all the subcomponents, the final correlation values are greater than 0.9 (in bold). Where this method really stands out for the optimal number of subcomponents is that when examining the highest correlation over all methods, using 2 subcomponents utilizes most hits over other methods. Therefore, during optimization 2 subcomponents will be used

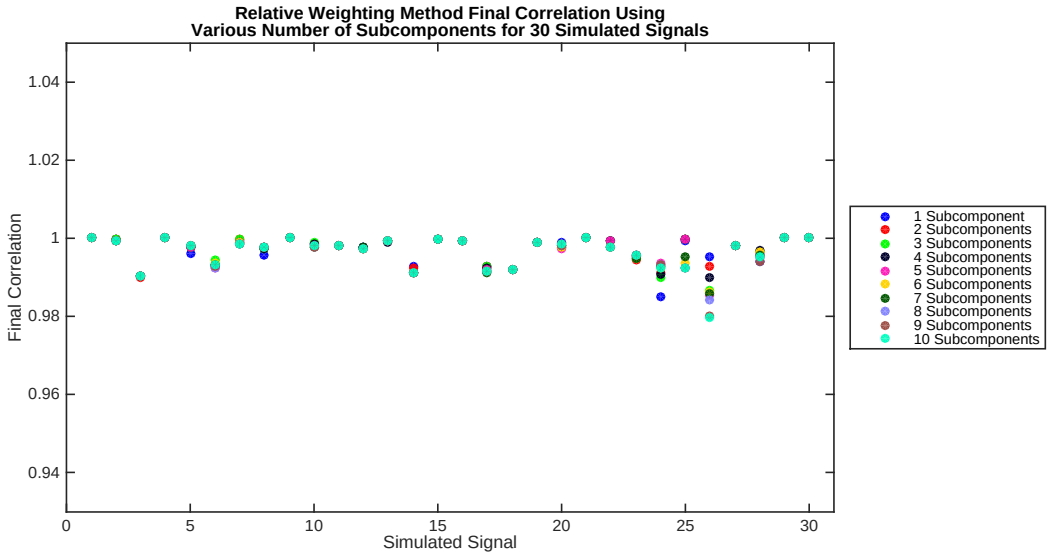

FIGURE 8.6: Output Correlation Values for Relative Weighting Prediction Algorithm for 1 to 10 Subcomponents used for Prediction of 30 Simulated Cases.

Table 8.3: Average and Standard Deviation of Prediction Final Correlations and RMSE, Correlation Classification, and Highest Correlation for 30 Simulated Cases for Approximate Full Respiratory Cycle using Various Number of Subcomponents for Relative Weighting Strategy.

Subcomponents	1	2	3	4	5	6	7	8	9	10
Average Correlation	**0.997**	**0.997**	**0.997**	**0.997**	**0.997**	**0.997**	**0.997**	**0.997**	0.996	0.996
St. Dev. Correlation	**0.004**	0.012	0.006	0.016	0.042	0.101	0.098	0.143	0.180	0.274
Average RMSE	**0.036**	**0.037**	**0.035**	0.038	0.043	0.045	0.047	0.047	0.047	0.048
St. Dev. RMSE	**0.031**	**0.031**	0.030	0.029	0.032	0.034	0.037	0.037	0.037	0.037
$cc \geqslant 0.9$	**30**	**30**	**30**	**30**	**30**	**30**	**30**	**30**	**30**	**30**
$0.5 \leqslant cc < 0.9$	0	0	0	0	0	0	0	0	0	0
$cc < 0.5$	0	0	0	0	0	0	0	0	0	0
Highest Correlation	0	**17**	15	13	**17**	16	**18**	**18**	**19**	**20**

8.2.3 Pattern Prediction

Figure 8.7 depicts the effect on final correlation coefficient by varying the number of optimal subcomponents using Pattern Prediction. This method demonstrates the most variation of final correlations. Simulations 23 was Baseline Shift followed by Noise and has the most spread in final correlation. Notice that the larger number of subcomponents used for this case, the worse the final correlation is. Table 8.4 is a summary of all averages and standard deviations of final correlations and RMSE values, as well as, information depicting where the correlations lie numerically, and which methods have the highest correlation for the given number of subcomponents versus other prediction methods. Notice that for pattern method, a maximum average correlation is obtained with 1 subcomponent with a small RMSE. Also, using 1 subcomponent 19 final correlation coefficients were greater than 0.9.

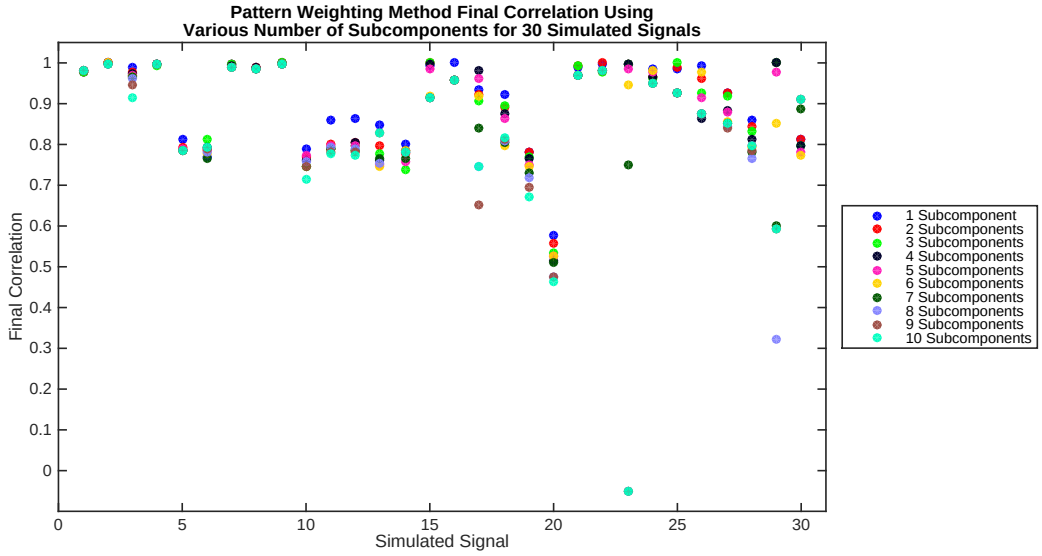

FIGURE 8.7: Output Correlation Values for Pattern Weighting Prediction Algorithm for 1 to 10 Subcomponents used for Prediction of 30 Simulated Cases.

Table 8.4: Average and Standard Deviation of Prediction Final Correlations and RMSE, Correlation Classification, and Highest Correlation for 30 Simulated Cases for Approximate Full Respiratory Cycle using Various Number of Subcomponents for Pattern Method.

Subcomponents	1	2	3	4	5	6	7	8	9	10
Average Correlation	**0.915**	0.902	0.895	0.890	0.887	0.875	0.855	0.816	0.823	0.823
St. Dev. Correlation	**0.104**	0.111	0.116	0.117	0.116	0.116	0.125	0.225	0.211	0.211
Average RMSE	**0.166**	0.221	0.262	0.288	0.327	0.347	0.359	0.374	0.384	0.395
St. Dev. RMSE	**0.115**	0.139	0.157	0.162	0.151	0.139	0.148	0.148	0.147	0.146
$cc \geqslant 0.9$	**19**	18	18	16	17	16	13	14	14	14
$0.5 \leqslant cc < 0.9$	11	12	12	14	13	14	17	13	14	14
$cc < 0.5$	0	0	0	0	0	0	0	3	2	2
Highest Correlation	**3**	2	2	1	1	1	0	0	0	0

8.2.4 Derivative Equal Weighting Prediction

Figure 8.8 depicts the effect on final correlation coefficient by varying the number of optimal subcomponents using Derivative Equal Weighting Prediction. Five cases have a noticeable drift in final correlation from 1. Simulation 14 has the most spread in correlation. Recall, from Equal Weighting Prediction that Signal 14 also had spreading in final correlation. Simulation Signal 14 was Regular Breathing followed

by Baseline Shift followed by a Periodicity Change. Notice that the larger number of subcomponents used for this case, the worse the final correlation is. Table 8.5 is a summary of all averages and standard deviations of final correlations and RMSE values, as well as, information depicting where the correlations lie numerically, and which methods have the highest correlation for the given number of subcomponents versus other prediction methods. Notice that for derivative equal weighting, a maximum average correlation with low average RMSE is obtained with 2 subcomponents (in bold), and when using 2 subcomponents, 28 of the simulations have predictions with the final correlation values are greater than 0.9.

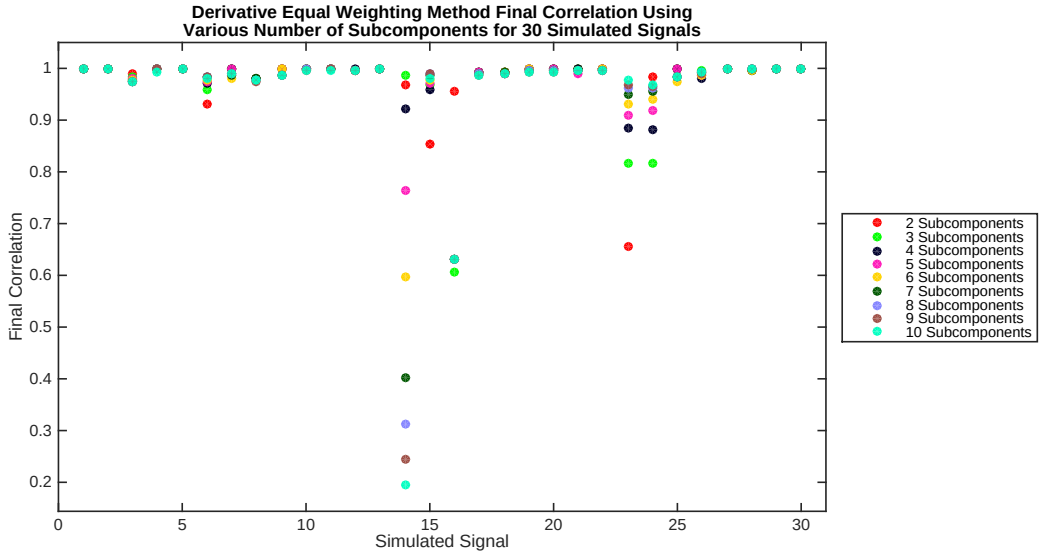

FIGURE 8.8: Output Correlation Values for Derivative Equal Weighting Prediction Algorithm for 2 to 10 Subcomponents used for Prediction of 30 Simulated Cases.

Table 8.5: Average and Standard Deviation of Prediction Final Correlations and RMSE, Correlation Classification, and Highest Correlation for 30 Simulated Cases for Approximate Full Respiratory Cycle using Various Number of Subcomponents for Derivative Equal Weighting Strategy.

Subcomponents	1	2	3	4	5	6	7	8	9	10
Average Correlation	N/A	**0.976**	0.969	0.972	0.969	0.964	0.959	0.956	0.954	0.952
St. Dev. Correlation	N/A	**0.068**	0.082	0.072	0.079	0.097	0.124	0.139	0.149	0.158
Average RMSE	N/A	**0.109**	0.112	0.107	0.113	0.123	0.131	0.133	0.141	0.152
St. Dev. RMSE	N/A	**0.137**	0.157	0.150	0.148	0.149	0.154	0.154	0.153	0.155
$cc \geqslant 0.9$	N/A	**28**	27	27	**28**	**28**	**28**	**28**	**28**	**28**
$0.5 \leqslant cc < 0.9$	N/A	2	3	3	2	2	1	1	1	1
$cc < 0.5$	N/A	0	0	0	0	0	1	1	1	1
Highest Correlation	N/A	0	2	4	1	3	3	2	1	1

8.2.5 Derivative Relative Weighting Prediction

Figure 8.9 depicts the effect on final correlation coefficient by varying the number of optimal subcomponents using Derivative Equal Weighting Prediction. While from this figure there is a noticeable drift in final correlation from 1 in many cases, notice that the y-axis ranges from 0.6 to 1.05. The most notable pattern is that both use of high (10) and low (1) number of subcomponents yield lower cross correlation. Table 8.6 is a summary of all averages and standard deviations of final correlations and RMSE values, as well as, information depicting where the correlations lie numerically, and which methods have the highest correlation for the given number of subcomponents versus other prediction methods. Notice that for derivative relative weighting, a maximum average correlation and low RMSE with small deviation is obtained with 5 subcomponents (in bold). Using 5 subcomponents, all of the final correlation values are greater than 0.9.

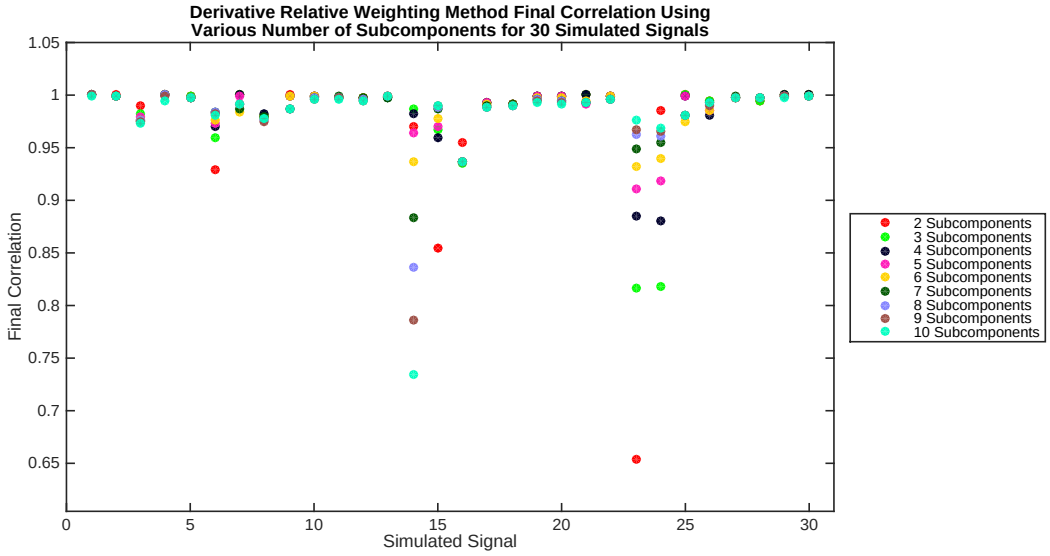

FIGURE 8.9: Output Correlation Values for Derivative Relative Weighting Prediction Algorithm for 2 to 10 Subcomponents used for Prediction of 30 Simulated Cases.

Table 8.6: Average and Standard Deviation of Prediction Final Correlations and RMSE, Correlation Classification, and Highest Correlation for 30 Simulated Cases for Approximate Full Respiratory Cycle using Various Number of Subcomponents for Derivative Relative Weighting Strategy.

Subcomponents	1	2	3	4	5	6	7	8	9	10
Average Correlation	N/A	0.976	0.980	0.984	**0.986**	0.982	0.985	0.984	0.982	0.980
St. Dev. Correlation	N/A	0.068	0.047	0.031	0.024	**0.021**	0.025	0.031	0.039	0.048
Average RMSE	N/A	0.109	0.105	0.098	**0.103**	0.111	0.113	0.114	0.121	0.129
St. Dev. RMSE	N/A	0.137	0.129	0.121	**0.117**	0.117	0.116	0.116	0.113	0.113
$cc \geqslant 0.9$	N/A	28	28	28	**30**	**30**	29	29	29	29
$0.5 \leqslant cc < 0.9$	N/A	2	2	2	0	0	1	1	1	1
$cc < 0.5$	N/A	0	0	0	0	0	0	0	0	0
Highest Correlation	N/A	5	4	3	**6**	3	2	0	1	1

Figure 8.10 demonstrates the summary of Figures 8.5 to 8.9. As highlighted by the boxes note that Equal Weighting has a maximum average correlation, $c = 0.997$ when using 1 Subcomponent (blue), Relative Weighting has a maximum average correlation, $c = 0.997$ when using 2 Subcomponents (red), Pattern Weighting has a maximum average correlation $c = 0.915$ when using 1 subcomponent (brown), Derivative Equal Weighting has a maximum average correlation $c = 0.976$ when

using 2 Subcomponents (black), and Derivative Relative Weighting has a maximum average correlation of $c = 0.976$ when using 5 Subcomponents (green). These number of subcomponents are considered in the optimization process.

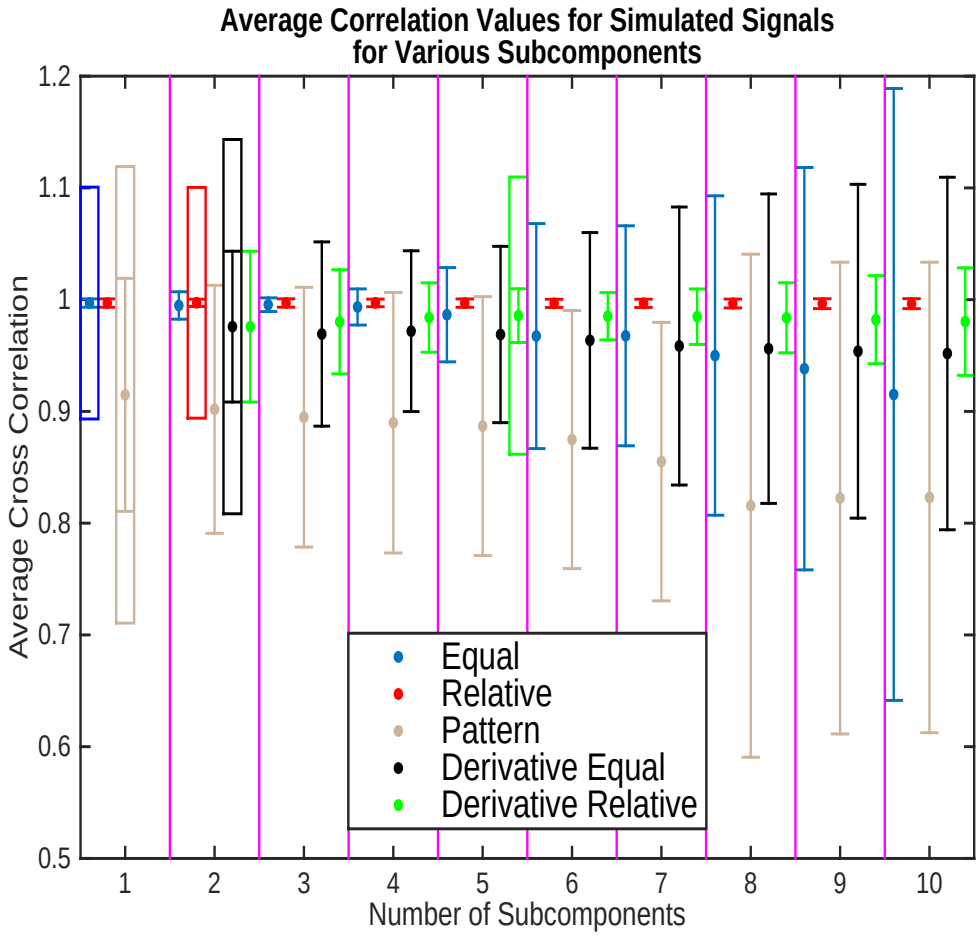

FIGURE 8.10: Optimal Number of Subcomponents used for Prediction for Each Prediction Method. The boxes represent the number of subcomponents with the highest average correlation coefficient with low deviations for the 30 simulations.

8.3 Effect of Full versus Half Respiratory Cycle

For the given algorithm the question arises of how far can we precisely predict accurately. These following results are performed to determine if a full or half respiratory cycle can be accurately predicted.

8.3.1 Simulated Signal Analysis for 5 Pt Moving Smoothing and Arbitrary Subcomponents

The simulated signals are sent into each of the five prediction algorithms described in Chapter 5 using a 5 point moving filter for smoothing and the number of subcomponents for a given prediction algorithm described in Chapter 4. The predictions were performed for an input and analysis component equal to approximately a full respiratory cycle and an approximate half respiratory cycle. Figure 8.11 illustrates the final predicted cross correlations between the prediction and analysis component. Notice that the scale for the full respiratory cycle prediction is from 0.3 to 1, whereas for the half it is much larger. There is less scattering for all algorithms aside from Pattern Prediction in the Half Respiratory Cycle Prediction. Notice that in general the spreading for each prediction algorithm is small for all algorithms aside from Pattern Prediction. Table 8.7 first describes the averages and standard deviations of the final correlation and RMSE for each prediction algorithm for full and half respiratory cycles. The table then classifies where each of the correlations lie for the simulations. Finally, Table 8.7 indicates which method yields the highest correlation for a given simulation. Notice that for both full and half respiratory cycles, Relative weighting yields 19 top correlations.

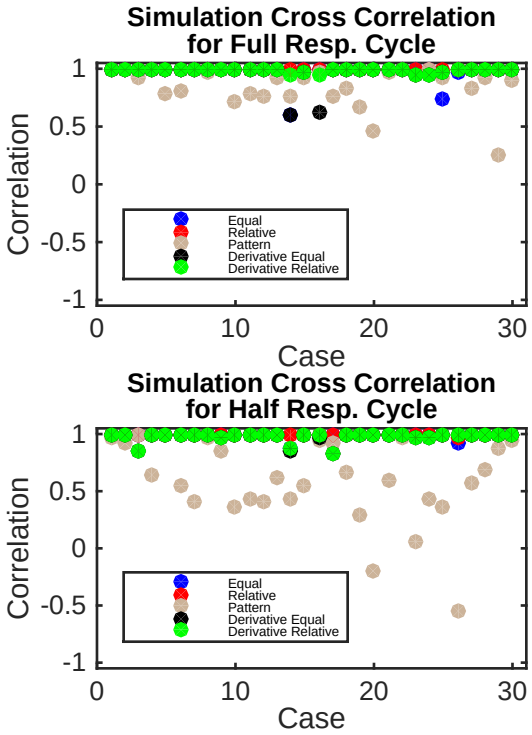

FIGURE 8.11: Scatter Plot of Correlation Values for full and half respiratory cycle prediction for 30 Simulated Cases. Using 5 Pt moving filter and arbitrary number of subcomponents.

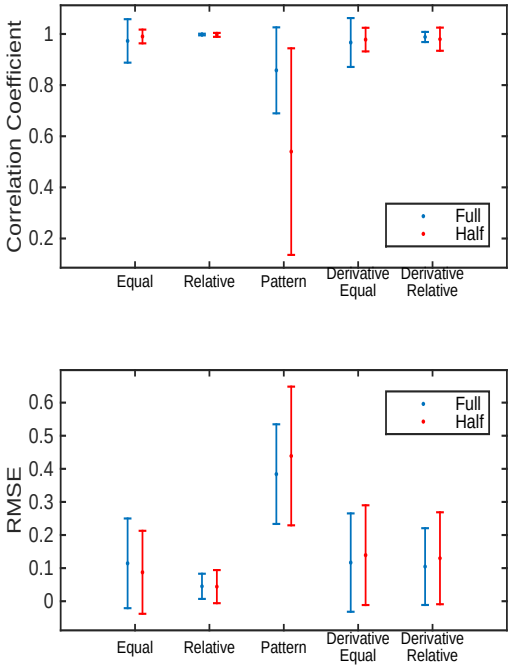

FIGURE 8.12: Average output correlation values and RMSE for full and half respiratory cycle prediction for 30 Simulated Signals using 5 Pt moving filter and arbitrary number of subcomponents.

Table 8.7: Summary of the averages and standard deviations for final correlation and RMSE, correlation classification and highest correlation values of 5 different prediction methods for approximate full and half respiratory cycle for 30 simulated cases. Using 5 Point Moving Filter and Arbitrary Number of Subcomponents

Method:	Equal		Relative		Pattern		Derivative Equal		Derivative Relative	
Cycle Length	Full	Half	Full	Half	Full	Half	Full	Half	Full	Half
Average Correlation	0.973	0.990	0.998	0.996	0.858	0.540	0.967	0.978	0.988	0.980
St. Dev. Correlation	0.085	0.027	0.003	0.008	0.168	0.404	0.096	0.046	0.020	0.045
Average RMSE	0.114	0.087	0.045	0.044	0.384	0.439	0.117	0.139	0.105	0.130
St. Dev. RMSE	0.135	0.125	0.038	0.050	0.151	0.209	0.149	0.151	0.116	0.139
$cc \geqslant 0.9$	28	29	30	30	17	8	28	27	30	27
$0.5 \leqslant cc < 0.9$	2	1	0	0	11	10	2	3	0	3
$cc < 0.5$	0	0	0	0	2	12	0	0	0	0
Highest Correlation	4	2	19	19	0	0	3	4	4	5

In Figure 8.12 the top plot represents the correlation average and standard deviation for a full respiratory cycle. Notice how close to 1 the value for Relative weighting is, with a value of 0.998 ± 0.003. For the half respiratory cycle prediction, the correlation coefficient values are all relatively close to 1, aside from the Pattern method. The bottom plot represents the RMSE for the full respiratory cycle. Notice that the value for the Relative weighting is close to 0, with a value of 0.045 ± 0.038. The RMSE values are similar for full and half respiratory cycle, aside from Pattern Method which has larger deviations for half respiratory cycle prediction.

8.3.2 Simulated Signal Analysis for 15 Pt S-G Smoothing and Arbitrary Subcomponents

The simulated signals are sent into each of the five prediction algorithms described in Chapter 5 using 15 point S-G filter for smoothing based on the results from Figure 8.3 and the number of subcomponents for a given prediction algorithm described in Chapter 4. The predictions were performed for an input and analysis component equal to approximately a full respiratory cycle and an approximate half respiratory cycle. Figure 8.13 illustrates the final predicted cross correlations between the prediction and analysis component. Notice that the scale for the full respiratory cycle prediction is from 0 to 1, whereas for the half it is much larger. There is less scattering for all algorithms aside from Pattern Prediction in the Half Respiratory Cycle Prediction. Notice that in general the spreading for each prediction algorithm is small for all algorithms aside from Pattern Prediction. Table 8.8 first describes the averages and standard deviations of the final correlation and RMSE for each prediction algorithm for full and half respiratory cycles. The table classifies where each of the correlations lies. Finally, Table 8.8 indicates which method yields the highest correlation for a given simulation. Notice that for full and half respiratory cycles, Relative weighting yields 17 and 18 top correlations, respectively.

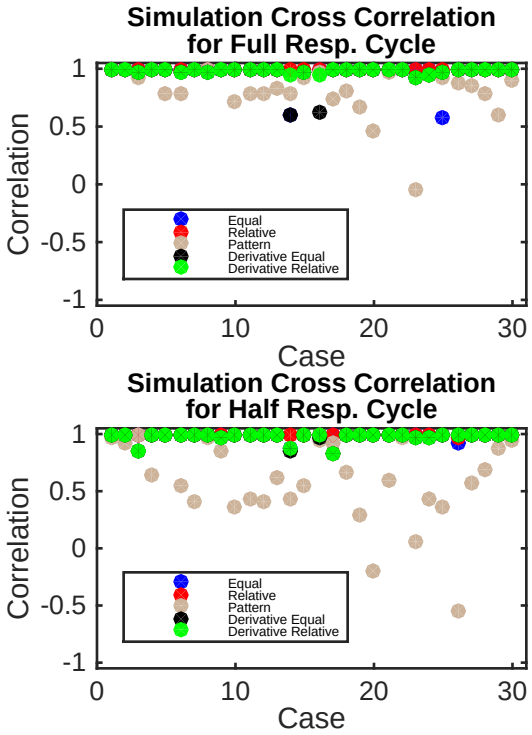

FIGURE 8.13: Scatter Plot of Correlation Values for full and half respiratory cycle prediction for 30 Simulated Cases. Using 15 Pt S-G Filter and arbitrary number of subcomponents.

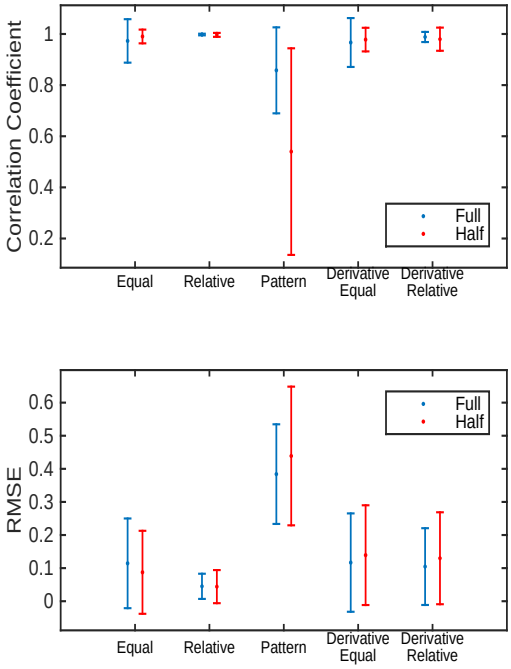

FIGURE 8.14: Average output correlation values and RMSE for full and half respiratory cycle prediction for 30 simulated signals using 15 Pt S-G filter and arbitrary number of subcomponents.

Table 8.8: Summary of the averages and standard deviations for final correlation and RMSE values of 5 different prediction methods for approximate full and half respiratory cycle for 30 simulated cases. 15 Point Savitzky-Golay Filter and arbitrary number of subcomponents were used.

Method:	Equal		Relative		Pattern		Derivative Equal		Derivative Relative	
Cycle Length	Full	Half	Full	Half	Full	Half	Full	Half	Full	Half
Average Correlation	0.967	0.989	0.997	0.994	0.823	0.568	0.964	0.974	0.985	0.976
St. Dev. Correlation	0.101	0.026	0.004	0.009	0.211	0.416	0.096	0.055	0.021	0.055
Average RMSE	0.115	0.095	0.045	0.052	0.395	0.440	0.123	0.149	0.111	0.139
St. Dev. RMSE	0.140	0.124	0.034	0.052	0.146	0.212	0.149	0.155	0.117	0.144
$cc \geqslant 0.9$	28	29	30	30	14	9	28	27	30	27
$0.5 \leqslant cc < 0.9$	2	1	0	0	14	9	2	3	0	3
$cc < 0.5$	0	0	0	0	2	12	0	0	0	0
Highest Correlation	7	2	17	18	0	1	3	2	3	7

In Figure 8.14 the top plot represents the correlation average and standard deviation for a full respiratory cycle. Notice how close to 1 the value for Relative weighting is with very small standard deviation, or 0.997 ± 0.004. Similarly, half respiratory cycle predictions have comparable correlation coefficient values to the full respiratory cycle, aside from Pattern Method. The bottom plot represents the RMSE for the full respiratory cycle. Notice that the value for the Relative weighting is close to 0, or 0.045 ± 0.034. The half cycle predictions are comparable to the full cycle predictions aside from the Pattern Method.

8.3.3 Simulated Signal Analysis for 15 Pt S-G Smoothing and Chosen Subcomponents

The simulated signals are sent into each of the five prediction algorithms described in Chapter 5 using 15 point S-G filter for smoothing based on the results from Figure 8.3 and the number of subcomponents for a given prediction algorithm based on the results from 8.10. The predictions were performed for an input and analysis component equal to approximately a full respiratory cycle and an approximate half respiratory cycle. Figure 8.15 illustrates the final predicted cross correlations between the prediction and analysis component. Notice that the scale for the full respiratory cycle prediction is from 0.5 to 1, whereas for the half it is much larger. There is less scattering for all algorithms aside from Pattern Prediction in the Half Respiratory Cycle Prediction. Table 8.9 first describes the averages and standard deviations of the final correlation and RMSE for each prediction algorithm for full and half respiratory cycles. The table then classifies where each of the correlations lie for the simulations. Finally, Table 8.9 indicates which method yields the highest correlation for a given simulation. Notice that for full and half respiratory cycles, Equal weighting yields 17 and 12 top correlations, respectively, which is the top method for these corrections.

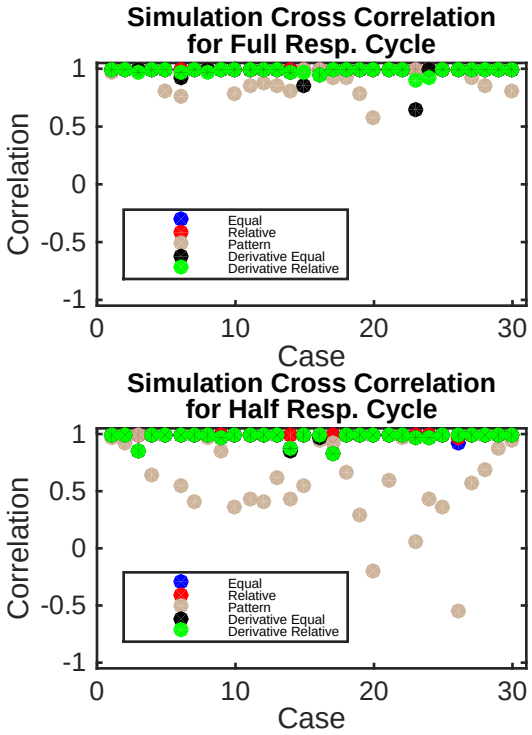

FIGURE 8.15: Scatter Plot of Correlation Values for each Prediction Algorithm for Full and Half Respiratory Cycle for 30 Simulated Cases. Using 15 Pt S-G Filter and respective optimal number of subcomponents.

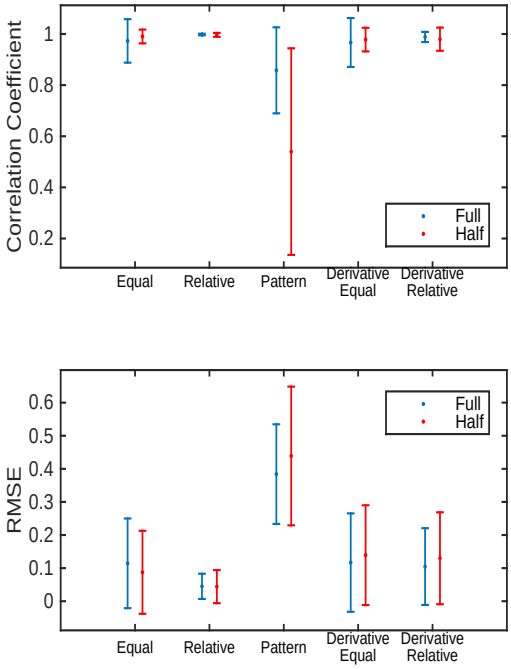

FIGURE 8.16: Average output correlation values and RMSE for full and half respiratory cycle prediction for 30 Simulated Signals using 15 Pt S-G filter and respective optimal number of subcomponents.

Table 8.9: Summary of the averages and standard deviations for final correlation and RMSE values of 5 different prediction methods for approximate full and half respiratory cycle for 30 simulated cases. 15 Point Savitzky-Golay Filter was used for smoothing for each prediction algorithm. The respective number of subcomponents were used as listed in the second row.

Method:	Equal		Relative		Pattern		Derivative Equal		Derivative Relative	
Subcomponents	1		2		1		2		5	
Cycle Length	Full	Half	Full	Half	Full	Half	Full	Half	Full	Half
Average Correlation	0.997	0.995	0.997	0.995	0.914	0.565	0.976	0.978	0.986	0.977
St. Dev. Correlation	0.004	0.006	0.003	0.007	0.104	0.555	0.067	0.052	0.024	0.052
Average RMSE	0.036	0.043	0.037	0.045	0.166	0.312	0.109	0.144	0.103	0.136
St. Dev. RMSE	0.031	0.037	0.031	0.041	0.115	0.276	0.137	0.134	0.117	0.134
$cc \geqslant 0.9$	30	30	30	30	19	12	28	28	30	28
$0.5 \leqslant cc < 0.9$	0	0	0	0	11	9	2	2	0	2
$cc < 0.5$	0	0	0	0	0	9	0	0	0	0
Highest Correlation	17	12	6	6	1	4	3	3	3	5

In Figure 8.16 the top plot represents the correlation and standard deviation for a full respiratory cycle. Both Equal and Relative Methods are close to 1 with very small deviations, 0.997 ± 0.004 and 0.995 ± 0.006, respectively. For half cycle prediction, aside from Pattern Method, all methods have values around 1 with small deviation. The bottom plot represents the RMSE values and deviations for each method for a full respiratory cycle. Again the Equal and Relative methods are close to 0 with small deviations, 0.036 ± 0.031 and 0.043 ± 0.037, respectively. For half cycle predictions, the Equal and Relative weighting methods perform better than the other methods in calculating RMSE values with small deviations close to 0, or 0.037 ± 0.031 and 0.045 ± 0.041, respectively.

8.3.4 Statistical Analysis of Simulated Signals

In order to determine differences as the algorithms are optimized and for full and half respiratory cycle predictions, a statistical analysis is performed. In Figure 8.17, the changes in cross correlation are displayed as changes are made to each algorithm for a full respiratory cycle. For instance, in each column is a particular algorithm and within the column the first box plot is using 5 Pt moving filter and arbitrary number of subcomponents for smoothing, the second column is 15 Pt S-G filter smoothing and arbitrary number of subcomponents, and the third column is 15 Pt S-G filter smoothing and optimal number of subcomponents applied. Figure 8.18 is similar for RMSE values for a full respiratory cycle for each algorithm. Figures 8.19 and 8.20 are plotted similarly for a half respiratory cycle.

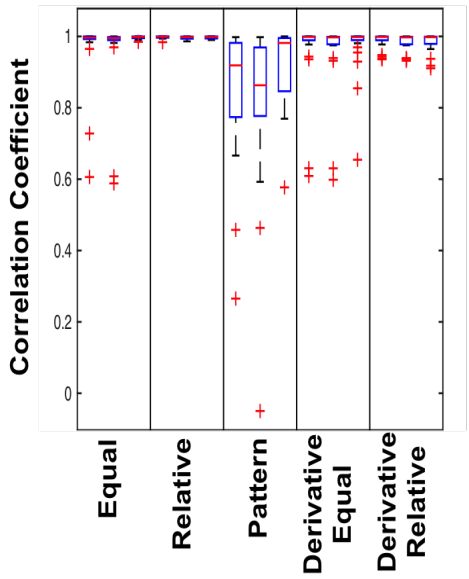

FIGURE 8.17: Changes in Cross Correlation for Algorithm Optimization for a Full Respiratory Cycle.

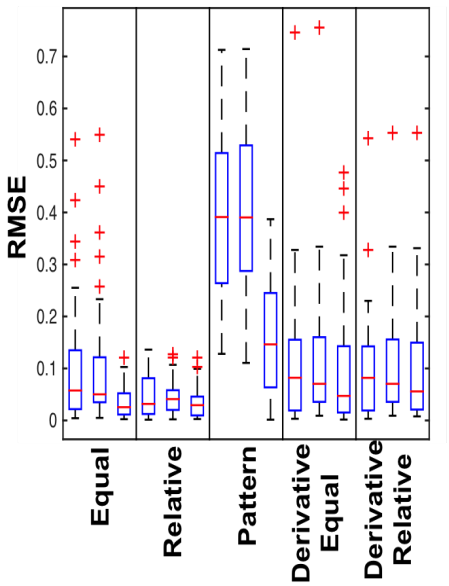

FIGURE 8.18: Changes in RMSE for Algorithm Optimization for a Full Respiratory Cycle.

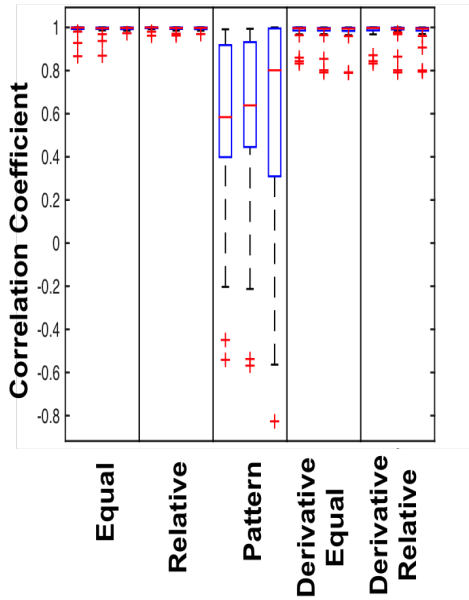

FIGURE 8.19: Changes in Cross Correlation for Algorithm Optimization for a Half Respiratory Cycle Prediction.

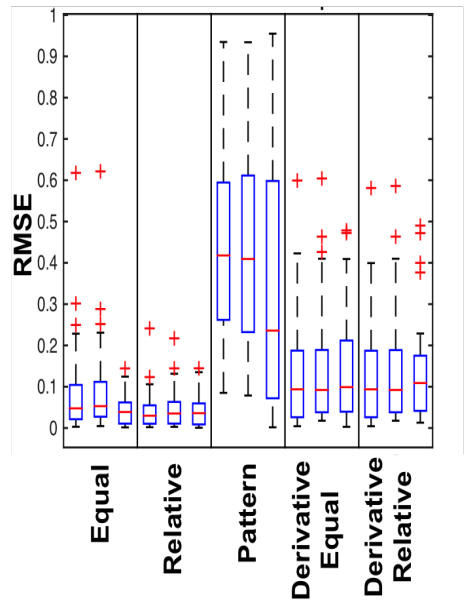

FIGURE 8.20: Changes in RMSE for Algorithm Optimization for a Half Respiratory Cycle.

In Figure 8.17, the spread of the final correlations for a full respiratory cycle prediction appears to decrease as they are optimized, have less outliers (red + signs), and generally move closer to 1, in all cases, except for Derivative Relative Method. Similarly, in Figure 8.18 the RMSE spreads for a full respiratory cycle prediction appears to decrease as the optimization is performed.

In Figure 8.19, the spread of the final correlations for a half respiratory cycle predictions appear to decrease for Equal and Relative Weighting Methods, with a decrease in outliers. Pattern Method appears to get worse as optimization is performed. The correlation values for Derivate Equal and Derivate Relative Weighting Methods appear to remain stable. In Figure 8.20, the spread of the RMSE values for a half respiratory cycle prediction for Equal and Relative Weighting appears to decrease, with a decrease in outliers. For Derivative Equal and Derivative Relative Weighting the spread is larger than those for Equal and Relative weighting, but not as large as that of Pattern Method.

8.3.5 Clinical Data for 5 Pt Moving Smoothing and Arbitrary Subcomponents

After optimization was performed, the prediction algorithms were applied to 555 patient and phantom data. The following is a representation of the prediction results for the 5 Pt moving filter and arbitrary chosen number of subcomponents for full and half cycle prediction. Table 8.10 first discusses the average and standard deviation of correlation coefficient and RMSE values. The table then categorizes where the correlation coefficient between the final prediction and analysis component lie. Finally, Table 8.10 determines which method has the highest correlation coefficient among the methods for a specified case.

Table 8.10: Summary of the averages and standard deviations for final correlation and RMSE values for full and half respiratory cycle predictions of clinical data using 5 Pt moving Filter and arbitrary number of subcomponents.

Method:	Equal		Relative		Pattern		Derivative Equal		Derivative Relative	
Cycle Length	Full	Half	Full	Half	Full	Half	Full	Half	Full	Half
Average Correlation	0.721	0.789	0.727	0.800	0.535	0.426	0.725	0.784	0.725	0.784
St. Dev. Correlation	0.390	0.398	0.383	0.385	0.454	0.562	0.397	0.389	0.398	0.389
Average RMSE	0.196	0.155	0.189	0.149	0.302	0.528	0.200	0.174	0.202	0.173
St. Dev. RMSE	0.174	0.171	0.161	0.138	0.162	0.179	0.169	0.150	0.181	0.149
$cc \geqslant 0.9$	260	359	259	363	121	22	281	350	281	349
$0.5 \leqslant cc < 0.9$	190	122	192	121	0	0	169	128	168	130
$cc < 0.5$	105	74	104	70	166	35	105	77	106	76
Highest Correlation	112	135	180	209	50	15	93	89	120	107

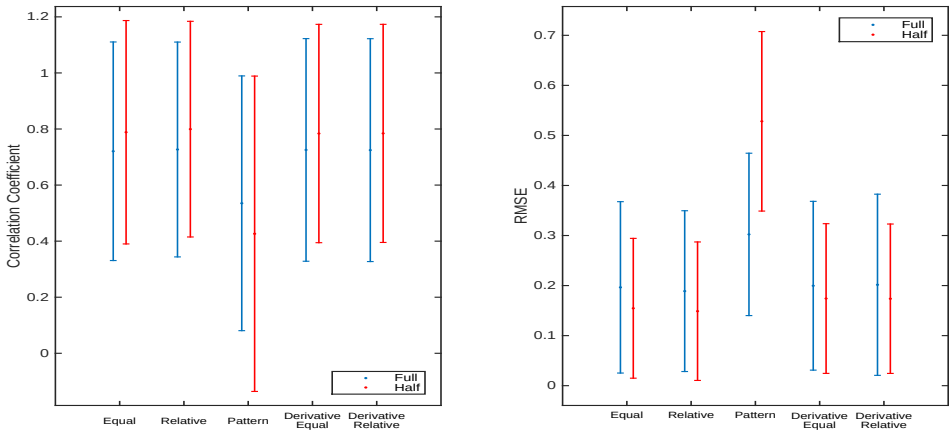

FIGURE 8.21: Average output correlation values and RMSE for full and half respiratory cycle of clinical data using 5 Pt moving filter and arbitrary number of subcomponents.

Figure 8.21 represents the averages and standard deviations of the correlation coefficient and RMSE values between the prediction and analysis component. Notice that for Equal, Relative, Derivative Equal and Derivative Relative the half cycle prediction correlation is higher than that of the full cycle. The half cycle values of these methods are 0.789 ± 0.398, 0.800 ± 0.385, 0.784 ± 0.389 and 0.784 ± 0.389, respectively. Similarly, for a half cycle prediction these methods yield a lower RMSE, with values of 0.189 ± 0.161, 0.149 ± 0.138, 0.174 ± 0.150, and 0.173 ± 0.149, respectively. Each of

these methods utilize average correlations and RMSE that are close to one another as demonstrated in Table 8.10. For Pattern method, the full cycle prediction does better than the half cycle, but the values are not close to the other methods. Notice that the half cycle prediction for Relative Weighting method yields the highest average correlation, with 363 *cc* values greater than 0.9, and 209 of the best correlations using this method which is the highest of any methods.

8.3.6 Clinical Data for 15 Pt S-G Smoothing and Arbitrary Subcomponents

The following is a representation of the prediction results for the 15 Pt S-G filter and arbitrary chosen number of subcomponents for full and half cycle prediction. Table 8.11 first discusses the average and standard deviation of correlation coefficient and RMSE values. The table categorizes where the correlation coefficient between the prediction and analysis component lie. Finally, Table 8.11 determines which method has the highest correlation coefficient among the methods for a specified case.

Table 8.11: Summary of the averages and standard deviations for final correlation and RMSE values for full and half respiratory cycle prediction of clinical data using 15 point S-G Filter and arbitrary number of subcomponents.

Method:	Equal		Relative		Pattern		Derivative Equal		Derivative Relative	
Cycle Length	Full	Half	Full	Half	Full	Half	Full	Half	Full	Half
Average Correlation	0.719	0.794	0.724	0.802	0.540	0.427	0.717	0.797	0.717	0.787
St. Dev. Correlation	0.393	0.390	0.389	0.384	0.444	0.557	0.407	0.382	0.407	0.382
Average RMSE	0.198	0.154	0.192	0.147	0.300	0.408	0.202	0.174	0.204	0.174
St. Dev. RMSE	0.174	0.142	0.164	0.139	0.165	0.199	0.173	0.151	0.185	0.150
$cc \geqslant 0.9$	264	360	260	366	121	20	277	347	277	347
$0.5 \leqslant cc < 0.9$	184	123	187	121	0	0	169	132	167	133
$cc < 0.5$	107	72	108	68	159	36	109	76	111	75
Highest Correlation	120	156	178	198	57	13	98	89	104	99

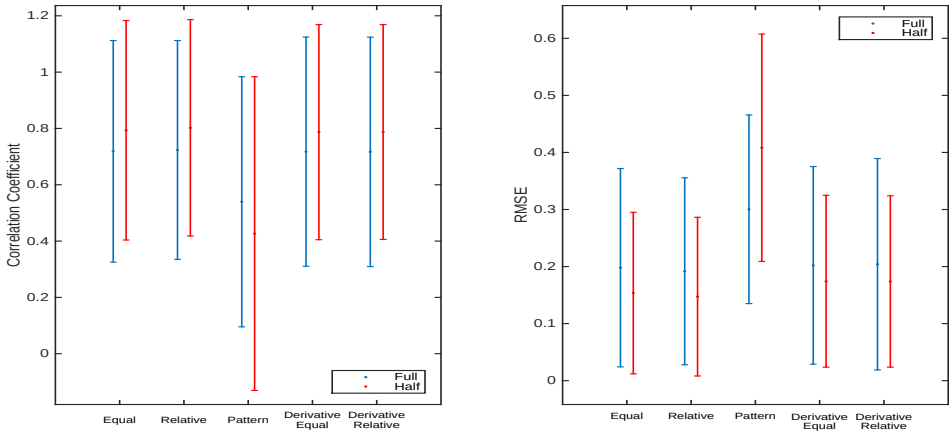

FIGURE 8.22: Average output correlation values and RMSE for full and half respiratory cycle prediction in clinical data using 15 Point S-G Filter and arbitrary number of subcomponents.

Notice that the averages and standard deviations for correlation coefficient and RMSE values appear similar to the 5 Pt moving filter with arbitrary number of subcomponents. The half cycle values of the Equal, Relative, Derivative Equal and Derivative Relative are highest for the half cycle and are 0.794 ± 0.390, 0.802 ± 0.384, 0.797 ± 0.382 and 0.787 ± 0.382, respectively. There are small changes that can be seen as improvements in Table 8.11. For instance, the average correlation increases very slightly for half cycle relative weighting prediction and the number of correlations greater than 0.9 increase, but there are fewer highest correlations than there were for the 5 Pt moving filter. In fact it is important to notice that all half cycle prediction average correlation coefficients increase slightly and the RMSE average values decrease slightly.

8.3.7 Clinical Data Analysis for 15 Pt S-G Smoothing and Chosen Subcomponents

The following is a representation of the prediction results for the 15 Pt S-G filter and chosen number of subcomponents based on Figure 8.10 for full and half cycle prediction. Table 8.12 first discusses the average and standard deviation of cor-

relation coefficient and RMSE values. The table categorizes where the correlation coefficient between the prediction and analysis component lie. Finally, Table 8.12 determines which method has the highest correlation coefficient among the methods for a specified case.

Table 8.12: Summary of the averages and standard deviations for final correlation and RMSE values for full and half respiratory cycle prediction of clinical data. 15 Point S-G Filter and the respective number of subcomponents were used as listed in the second row.

Method:	Equal		Relative		Pattern		Derivative Equal		Derivative Relative	
Subcomponents	1		2		1		2		5	
Cycle Length	Full	Half	Full	Half	Full	Half	Full	Half	Full	Half
Average Correlation	0.633	0.753	0.688	0.791	0.485	0.363	0.690	0.763	0.716	0.794
St. Dev. Correlation	0.455	0.422	0.415	0.390	0.491	0.609	0.428	0.406	0.408	0.372
Average RMSE	0.231	0.178	0.208	0.156	0.320	0.354	0.210	0.287	0.204	0.174
St. Dev. RMSE	0.204	0.177	0.180	0.152	0.208	0.214	0.180	0.166	0.185	0.150
$cc \geqslant 0.9$	244	323	257	352	113	15	265	116	274	345
$0.5 \leqslant cc < 0.9$	151	149	174	125	115	11	160	124	178	142
$cc < 0.5$	160	83	124	78	171	25	129	90	102	68
Highest Correlation	116	135	130	178	50	8	130	116	128	118

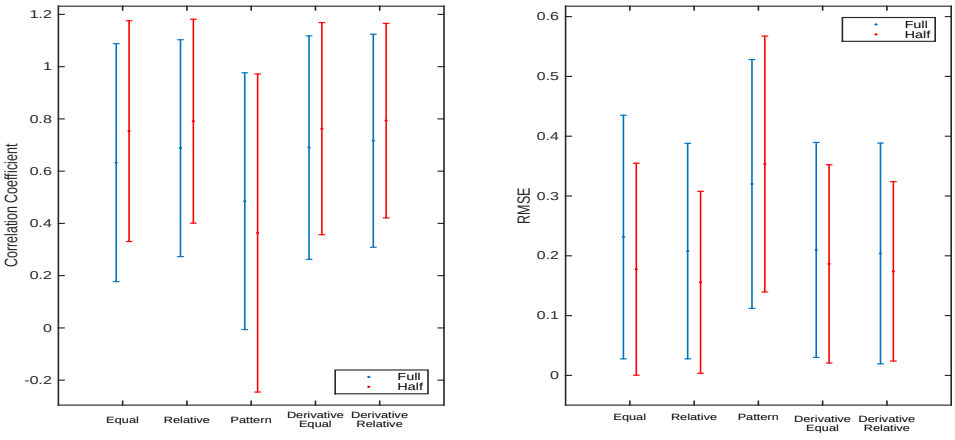

FIGURE 8.23: Average output correlation values and RMSE for full and half respiratory cycle prediction using clinical data. 15 Point S-G Filter and the respective number of subcomponents were used as listed in the second row.

In Figure 8.23 the left plot represents the correlation and standard deviation for a full and half respiratory cycle. Equal, Relative, Derivative Equal, and Derivative Relative

Methods are yield values close to 0.8 for the half cycle prediction, 0.753 ± 0.422 and 0.791 ± 0.390, 0.763 ± 0.406, and 0.794 ± 0.372 respectively. The right plot represents the RMSE values and deviations for each method for full and half respiratory cycle. Here the Equal, Relative and Derivative Relative methods for half cycle prediction are closest to 0, 0.178 ± 0.177, 0.156 ± 0.152, and 0.174 ± 0.150, respectively. Notice that for both the correlation and RMSE averages they begin to drift further from 1 and 0, respectively giving an indication that the number of subcomponents was not optimal for clinical data.

8.3.8 Statistical Analysis of Clinical Data

In order to determine if the optimization improved the predictions, box plots displaying correlation coefficient and RMSE were made to depict the data as optimizations were made. In Figure 8.24, correlation coefficient for full cycle prediction is depicted. For a given algorithm, the first box plot is the evaluation for 5 Pt moving filter and arbitrary number of subcomponents for prediction; the second box plot is the 15 Pt S-G filter and arbitrary number of subcomponents for prediction; and the third box plot is the 15 Pt S-G filter and chosen number of subcomponents for prediction. Similarly, in Figure 8.25, are the RMSE values for full cycle prediction. Figures 8.26 and 8.27 depict the correlation coefficient for half cycle prediction.

While there is a large amount of information depicted in these four plots, the key piece of data obtained from the plots is that the distributions of the correlation coefficient seem to move away from 1 as the optimization continues. There is a similar behavior in the RMSE values which have distributions moving away from 0 as optimization occurs. Therefore, in order to make a comparison, an examination of the 5 Pt moving filter and arbitrary chosen number of subcomponents will be used for evaluation of full and half cycle prediction.

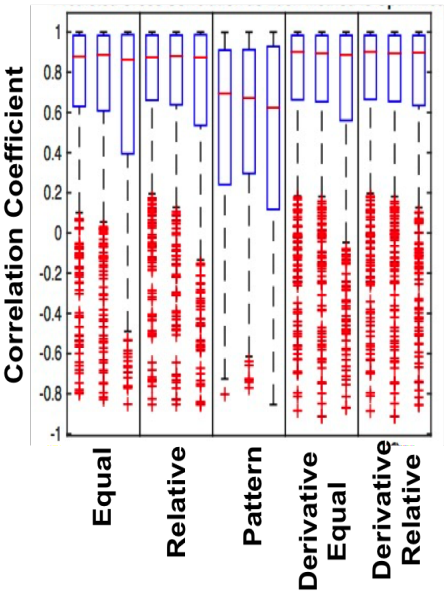

FIGURE 8.24: Changes in Clinical Data Correlation Coefficient for Algorithm Optimization for Full Cycle Prediction

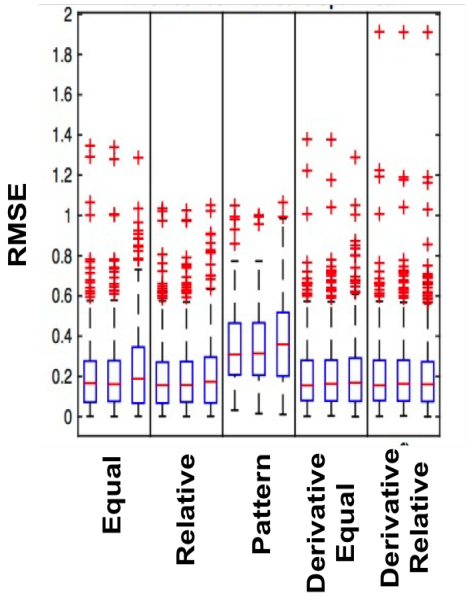

FIGURE 8.25: Changes in Clinical Data RMSE for Algorithm Optimization for Full Cycle Prediction

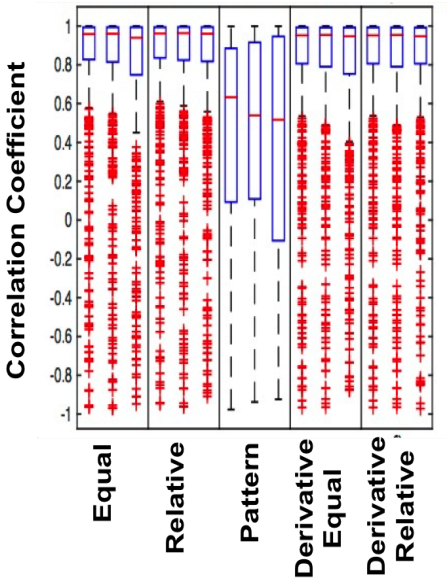

FIGURE 8.26: Changes in Clinical Data Correlation Coefficient for Algorithm Optimization for Half Cycle Prediction

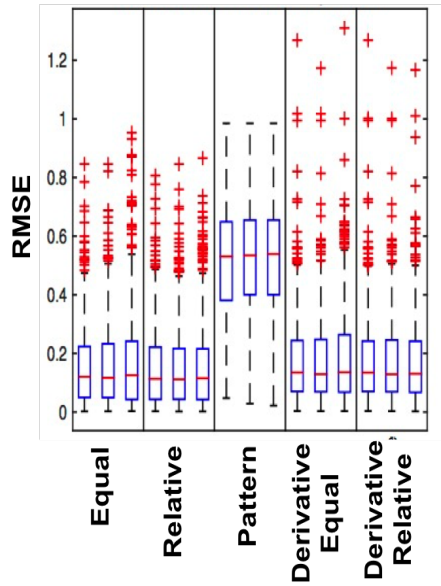

FIGURE 8.27: Changes in Clinical Data RMSE for Algorithm Optimization for Half Cycle Prediction

Figure 8.28 compares the distribution of correlation coefficient values from the full cycle (first column within a given algorithm) and half cycle (second column within a given algorithm) prediction for the 5 Pt moving filter and arbitrary number of subcomponents. Similarly, Figure 8.29 displays a comparison of the RMSE values from full and half cycle predictions. Notice that the distribution of half cycle predictions for most methods for both correlation coefficient and RMSE appear closer to 1 and 0, respectively, indicating better predictions when performing the half cycle prediction. Pattern method has a better distribution for full cycle predictions, but its correlation coefficient and RMSE values are not as optimal as the other methods.

Table 8.13 describes the results of a Wilcoxon signed-rank test on the full and half cycle prediction data. The test demonstrates that the correlation coefficient results are statistically significant in 4 out of the 5 algorithms (all but Pattern Method) in favor of the half cycle prediction. Similarly, these same 4 algorithms have a statistically significant RMSE in favor of the half cycle prediction.

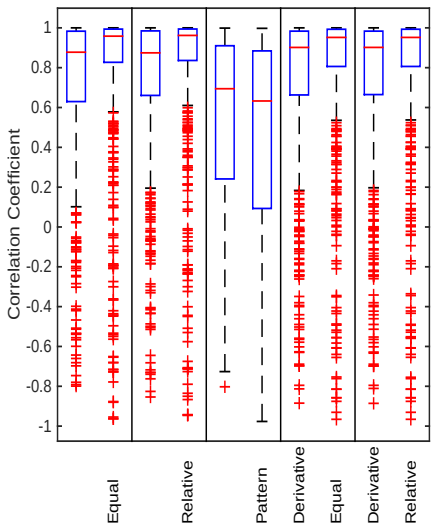

FIGURE 8.28: Changes in correlation coefficient values for 5 Pt moving filter and arbitrary number of subcomponents for full and half cycle predictions for clinical data.

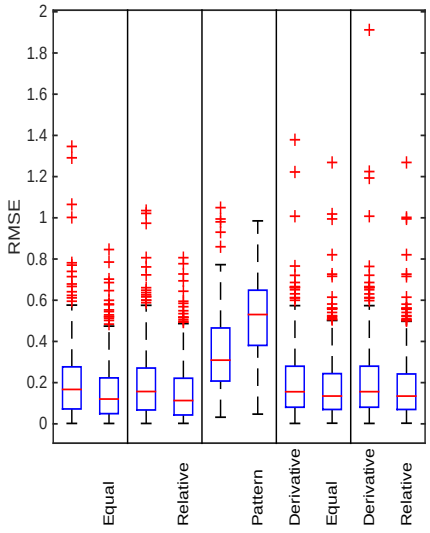

FIGURE 8.29: Changes in RMSE values for 5 Pt moving filter and arbitrary number of subcomponents for full and half cycle predictions for clinical data.

Table 8.13: Wilcoxon Signed-Rank test between full and half respiratory cycle correlation coefficient and RMSE for 5 Pt moving filter and arbitrary number of subcomponents for clinical data.

Method:	*cc* p-test	RMSE p-test
Equal	9×10^{-10}	2×10^{-13}
Relative	3×10^{-10}	1×10^{-12}
Pattern	0.330	0
Derivative Equal	9×10^{-7}	2×10^{-4}
Derivative Relative	4×10^{-7}	2×10^{-4}

9

Conclusions and Discussion

9.1 Conclusions

In conclusion, the number of subcomponents used for prediction may be better determined based on individual breathing pattern. The prediction accuracy using patient data is better using half cycle prediction over full cycle prediction for all algorithms for the majority of methods tested. Finally, relative weighting method performed better than other methods.

9.2 Discussion

In general, it is difficult to make evaluations of how patient data behaves. While we can simulate many different types of predictions, patients are unpredictable on a day to day basis making prediction difficult. Another important note is that in the future, simulation data should be generated with the same resolution in order to be able to apply all prediction corrections accurately. For instance, because the resolution was too low in the simulation data, the phase shift correction could not be applied. Based strictly on the 30 simulation cases, it is hard to determine if there

is a real improvement based on changing the length of prediction. Therefore, in the future a specific examination of a clinical database should be performed. Alternatively, a move towards individualized patient prediction will be necessary.

9.2.1 Data Preprocessing

Recall that the original algorithms, prior to any optimization, all utilized a 5 point moving filter. Upon reviewing the results using the various filters, Savitzky-Golay reduces noisy signals, but can maintain the integrity of simulated signals best. Figure 8.3 demonstrates that using the summed difference parameter using a Savitzky-Golay 15 Point Smoothing Filter gave the lowest change in correlation between the 30 Simulated Signals and their corresponding smoothed signals. Therefore, a 15 Point Savitzky-Golay Filter was used for algorithm optimization throughout the prediction algorithm.

While these were only some of the filters that can be used to smooth the data, future work might investigate 10% of the a respiratory cycle as the number point spans for a given filter, such that if the signal sampling rate were to change the smoothing would not be affected as it would then be a dynamic smoothing performance.

9.2.2 Coefficient of Similarity

Equation 4.6 demonstrates a non-linear combination of metrics used to determine optimal subcomponents which demonstrate similarities between themselves and the input component. Additionally, linear combination searching for similarities between the input component and subcomponents used only cross correlation. While these methods appeared to be effective in making prediction, these are only two ways to determine the optimal subcomponents. However, in the future other methods could

be considered.

9.2.3 Effect of Number of Subcomponents Used

In general, for each of the methods, as the number of subcomponents was increased, the final correlation between analysis component and prediction decreased, while the RMSE increased. One other important effect to note is that when we change the number of subcomponents we can significantly change the composition of the algorithm. For instance for Equal and Pattern weighting, when using 1 subcomponent, the algorithm no longer uses an average as the final step. This means that the effects of a potentially suboptimal signal cannot be overcome by the algorithm, leaving one with a suboptimal prediction. Additionally, examination of clinical data using weighting with heavier emphasis on more recent cycles should be considered in the future.

Another factor which could effect the outcome of the prediction is how the respiratory cycle length is determined. Currently, the algorithm averages determines a respiratory cycle over the entire data set, but considering the most recent data may be preferential. For instance, when a patient has a periodicity change, then the most recent breathing pattern will have a respiratory cycle of different length than the entire data. Therefore, considering a smaller portion when calculating the respiratory cycle should be considered.

If a patient has a sudden breathing change such as a cough or sneeze, then the algorithm should be robust to overcome this behavior, because of its identification process determining similarities between the input component and subcomponents. This is true when there is sufficient data for subcomponent matching, i.e. the data is several respiratory cycles long. Clinically, it is questioned whether using the total data set or the most recent data set should be used for improved prediction.

Performing a quick examination of the prediction algorithms showed that using the total data set was optimal in several cases, again because the algorithm identifies only similar components. However, this could be easily effected by changing the number of subcomponents used for prediction and altering the separation size requirement between top-ranked subcomponents. As demonstrated by clinical data, using less subcomponents for prediction did not improve the prediction. There likely is an ideal number to use but this would need to be determined using a clinical database or moving toward individualized patient determination.

9.3 Effect of Full versus Half Respiratory Cycle Prediction

The half respiratory cycle prediction clearly performed better in 4 out of 5 algorithms (Equal, Relative, Derivative Equal, and Derivative Relative Weighting) for clinical data. Both the distributions and the statistical significance rules in favor of a half cycle prediction over a full cycle prediction. This seems reasonable, because the longer the desired prediction is, the harder it is to find data that is similar to the input. In the event that another prediction length is to be determined, such as a quarter, one and a quarter or one and a half respiratory cycles, it appears that as the data is lengthened the prediction accuracy will decrease. In other words, the quarter respiratory cycle will likely perform better than a half respiratory cycle prediction, and one and a quarter or one and a half respiratory cycles will be less accurate than a full respiratory cycle prediction.

9.3.1 Future Work

A few steps would need to be taken in order to implement the prediction algorithm clinically. First, the algorithm would have to be altered to predict dynamically. The computational time to make prediction would need to be accounted for and added to required prediction length. At the current state, the algorithm takes on average less

than 2 seconds to form a prediction. Additionally, to keep the predictions in check some sort of feedback should be added to the algorithm. The feedback could be an imaging based method or a certain threshold around the respiratory trace signal or some combination of the two. Imaging verification to ensure that the tumor is actually following surrogate signals. For instance CBCT or fluoroscopy methods could be used to verify the motion. Another method of verification is using a threshold of the prediction from the surrogate motion. Vendors such as Varian add a deviation around the respiratory trace that forces their learning algorithm to recalculate when the threshold is exceeded. A similar metric that is used in this algorithm is the RMSE value, which could have a threshold placed on it. However, when placing this threshold mechanism on the data, the algorithm moves more towards a NN in that it would need some sort of optimization performed when it exceeds the threshold or alternatively would need the patient to be coached more.

Bibliography

[1] F. M. Khan, *The physics of radiation therapy.* Lippincott Williams & Wilkins, 2010.

[2] J. Cai, Z. Chang, J. ODaniel, S. Yoo, H. Ge, C. Kelsey, and F.-F. Yin, "Investigation of sliced body volume (sbv) as respiratory surrogate," *Journal of Applied Clinical Medical Physics*, vol. 14, no. 1, 2013.

[3] Q. Ren, S. Nishioka, H. Shirato, and R. I. Berbeco, "Adaptive prediction of respiratory motion for motion compensation radiotherapy," *Physics in medicine and biology*, vol. 52, no. 22, p. 6651, 2007.

[4] H. Yan, F.-F. Yin, G.-P. Zhu, M. Ajlouni, and J. H. Kim, "The correlation evaluation of a tumor tracking system using multiple external markers," *Medical physics*, vol. 33, no. 11, pp. 4073–4084, 2006.

[5] N. Fukumitsu, T. Hashimoto, T. Okumura, M. Mizumoto, E. Tohno, K. Fukuda, M. Abei, T. Sakae, and H. Sakurai, "Investigation of the geometric accuracy of proton beam irradiation in the liver," *International Journal of Radiation Oncology Biology Physics*, vol. 82, no. 2, pp. 826–833, 2012.

[6] V. R. Kini, S. S. Vedam, P. J. Keall, S. Patil, C. Chen, and R. Mohan, "Patient training in respiratory-gated radiotherapy," *Medical Dosimetry*, vol. 28, no. 1, pp. 7–11, 2003.

[7] P. J. Keall, G. S. Mageras, J. M. Balter, R. S. Emery, K. M. Forster, S. B. Jiang, J. M. Kapatoes, D. A. Low, M. J. Murphy, B. R. Murray, *et al.*, "The management of respiratory motion in radiation oncology report of aapm task group 76a," *Medical physics*, vol. 33, no. 10, pp. 3874–3900, 2006.

[8] I. Vergalasova, J. Cai, and F.-F. Yin, "A novel technique for markerless, self-sorted 4d-cbct: Feasibility study," *Medical physics*, vol. 39, no. 3, pp. 1442–1451, 2012.

[9] G. C. Sharp, S. B. Jiang, S. Shimizu, and H. Shirato, "Prediction of respiratory tumour motion for real-time image-guided radiotherapy," *Physics in medicine and biology*, vol. 49, no. 3, p. 425, 2004.

[10] S. Hong, B. Jung, and D. Ruan, "Real-time prediction of respiratory motion based on a local dynamic model in an augmented space," *Physics in medicine and biology*, vol. 56, no. 6, p. 1775, 2011.

[11] S. Ahn, B. Yi, Y. Suh, J. Kim, S. Lee, S. Shin, and E. Choi, "A feasibility study on the prediction of tumour location in the lung from skin motion," 2014.

[12] A. E. Torshabi, M. Riboldi, A. A. I. Fooladi, S. M. M. Mosalla, and G. Baroni, "An adaptive fuzzy prediction model for real time tumor tracking in radiotherapy via external surrogates," *Journal of Applied Clinical Medical Physics*, vol. 14, no. 1, 2013.

[13] H. Yan, F.-F. Yin, G.-P. Zhu, M. Ajlouni, and J. H. Kim, "Adaptive prediction of internal target motion using external marker motion: a technical study," *Physics in medicine and biology*, vol. 51, no. 1, p. 31, 2006.

[14] M. Seregni, A. Pella, M. Riboldi, R. Orecchia, P. Cerveri, and G. Baroni, "Real-time tumor tracking with an artificial neural networks-based method: A feasibility study," *Physica Medica*, vol. 29, no. 1, pp. 48–59, 2013.

[15] F. Ernst and A. Schweikard, "Predicting respiratory motion signals for image-guided radiotherapy using multi-step linear methods (mulin)," *International Journal of Computer Assisted Radiology and Surgery*, vol. 3, no. 1-2, pp. 85–90, 2008.

[16] A. Schweikard, H. Shiomi, and J. Adler, "Respiration tracking in radiosurgery," *Medical physics*, vol. 31, no. 10, pp. 2738–2741, 2004.

[17] D. Yang, J. Cao, J. Fu, J. Wang, and J. Guo, "A pattern fusion model for multi-step-ahead cpu load prediction," *Journal of Systems and Software*, vol. 86, no. 5, pp. 1257–1266, 2013.

[18] I. Varian Medical Systems, "Specifications real-time position management system," August 2007.

[19] I. Varian Medical Systems, "Real-time position management system," August 2007.

[20] Mathworks, "Filtering and smoothing data," *Matlab2014b*, 2014.

[21] W. H. Press and S. A. Teukolsky, "Savitzky-golay smoothing filters," *Computers in Physics*, vol. 4, no. 6, pp. 669–672, 1990.

[22] Q. Wu and S. Das, "Lecture 6: Feature-based image registartion: Contour-based matching." 2014.

[23] I. Zawisza, H. Yan, and F. Yin, "Su-c-brf-07: A pattern fusion algorithm for multi-step ahead prediction of surrogate motion," *Medical Physics*, vol. 41, no. 6, pp. 98–98, 2014.